

SCIENTIFIC REPORTS

OPEN

Cristae remodeling causes acidification detected by integrated graphene sensor during mitochondrial outer membrane permeabilization

Ted D. Pham¹, Phi Q. Pham², Jinfeng Li², Anthony G. Letai³, Douglas C. Wallace⁴ & Peter J. Burke^{1,2,5}

Received: 23 March 2016
Accepted: 07 October 2016
Published: 27 October 2016

The intrinsic apoptotic pathway and the resultant mitochondrial outer membrane permeabilization (MOMP) via BAK and BAX oligomerization, cytochrome c (cytc) release, and caspase activation are well studied, but their effect on cytosolic pH is poorly understood. Using isolated mitochondria, we show that MOMP results in acidification of the surrounding medium. BAK conformational changes associated with MOMP activate the OMA1 protease to cleave OPA1 resulting in remodeling of the cristae and release of the highly concentrated protons within the cristae invaginations. This was revealed by utilizing a nanomaterial graphene as an optically clear and ultrasensitive pH sensor that can measure ionic changes induced by tethered mitochondria. With this platform, we have found that activation of mitochondrial apoptosis is accompanied by a gradual drop in extra-mitochondrial pH and a decline in membrane potential, both of which can be rescued by adding exogenous cytc. These findings have importance for potential pharmacological manipulation of apoptosis, in the treatment of cancer.

The intrinsic mitochondrial pathway of apoptosis is an important target for pharmacological manipulation for a variety of diseases including cancer^{1–7}. This pathway is regulated by the BCL-2 family proteins⁸ and results in the collapse of the inner membrane electrochemical gradient. An early step in the initiation of the intrinsic apoptosis pathway is the mitochondrial outer membrane permeabilization (MOMP). MOMP can be induced by BH3-only proteins such as tBid and BIM and has been proposed to result from the oligomerization of pro-apoptotic BCL-2 family proteins BAX and BAK⁸. BAX and BAK oligomerization activates the metalloprotease, OMA1, to cleave the inner membrane protein OPA1⁹. OPA1 tethers the inner membrane cristae loops together at cristae junctions creating the inter-cristae luminal spaces into which the electron transport chain pumps protons during oxidative phosphorylation (OXPHOS)¹⁰. Cleavage of OPA1 results in remodeling of the cristae and the opening of the proton-rich cristae luminal spaces^{9,11}. MOMP permits the release of stored inter-membrane space pro-apoptotic proteins including cytochrome c (cytc), procaspase-9, and Smac/DIABLO into the cytoplasm, causing activation of caspases and the commitment to cell death.

It has been reported that the cytosol becomes acidified soon after the intrinsic apoptosis pathway is activated^{12–14}. However, there has not been a method to quantify and thus understand the molecular and physiological basis of this phenomenon.

Here, we present an electronic method to detect extra-mitochondrial pH of isolated mitochondria, based on tethering the mitochondria to one-atom thin graphene. The mitochondria are tethered via graphene bound antibodies which recognize the mitochondrial outer membrane protein, TOM20. Graphene is an excellent conductor

¹Department of Biomedical Engineering, University of California, Irvine, CA, USA. ²Department of Chemical Engineering and Materials Science, University of California, Irvine, CA, USA. ³Dana-Farber Cancer Institute, Harvard University, Boston, MA, USA. ⁴Center for Mitochondrial and Epigenomic Medicine, Children's Hospital of Philadelphia and Department of Pathology and Laboratory Medicine, University of Pennsylvania, Philadelphia, PA, USA. ⁵Department of Electrical Engineering and Computer Science, University of California, Irvine, CA, USA. Correspondence and requests for materials should be addressed to P.J.B. (email: pburke@uci.edu)

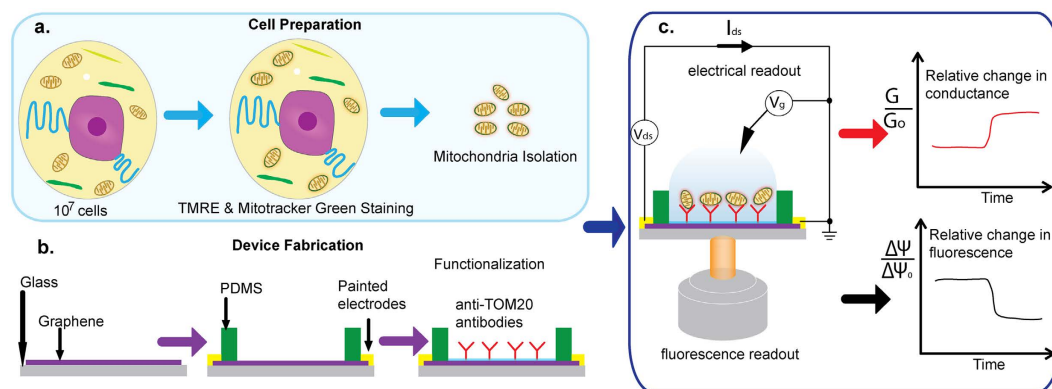


Figure 1. Overview of the experimental workflow. (a) Mitochondria are isolated on the day of experimentation and loaded on (b) a pre-functionalized device. (c) After a brief incubation, mitochondrial functions can be probed via electrical and fluorescent methods.

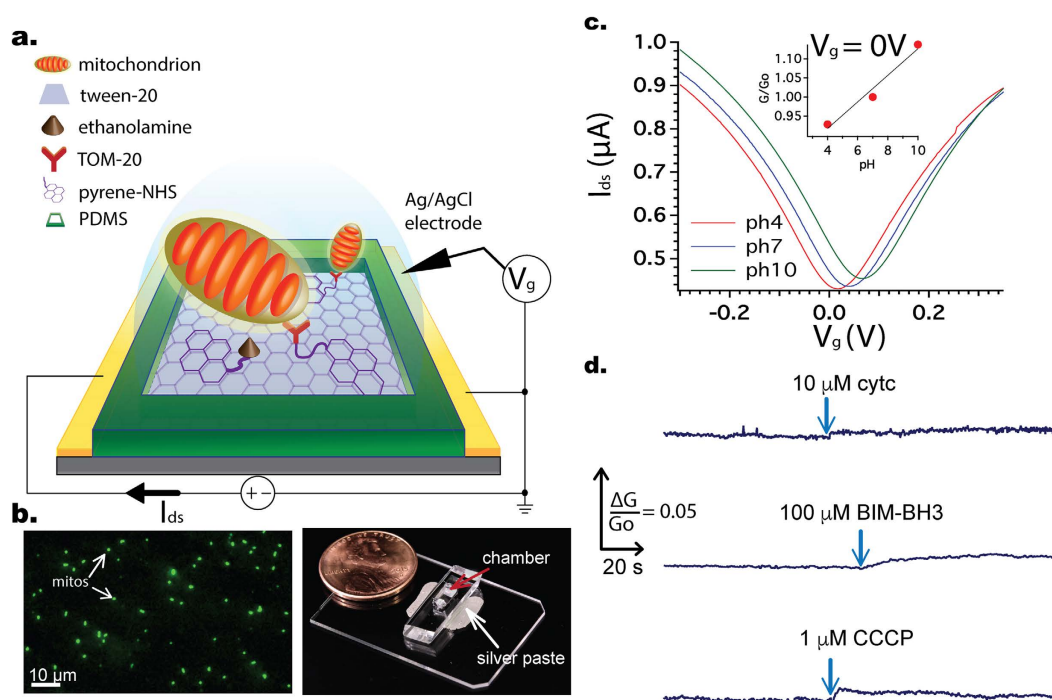


Figure 2. (a) Overview of the functionalization scheme (Mitochondria not to scale); (b) Immobilized mitochondria (from HeLa cells) on functionalized graphene surface, false colored from 100 nM MitoTracker® Green FM signals. A finished graphene-on-glass device; graphene is at the bottom of the chamber indicated by the red arrow; (c) I_{ds} vs V_g (electrolyte gate) characteristics with different pH KCl buffers; (d) Insignificant fluctuations of graphene conductance following the additions of various substrates.

and changes in the pH surrounding the mitochondria can change the graphene conductance and be detected electrically. Being optically transparent, the graphene layer also permits optical interrogation of the mitochondria^{15–17} concurrent with analysis of ionic changes. Hence, our system permits the simultaneous monitoring of changes in extra-mitochondrial pH through graphene conductance and inner membrane potential ($\Delta\Psi_m$) using the potentiometric fluorescent dye tetramethylrhodamine ethyl ester perchlorate (TMRE).

Results

An overview of our experimental system is shown in Fig. 1. After the graphene device is fabricated and prepared, purified mitochondria can be tethered to the anti-TOM20 antibodies. The graphene conductance then permits the electronic detection of mitochondrial ion exchange and the optical properties of the graphene permit the staining and visualization of the mitochondrial membrane potential.

We used a bottom-up approach to deposit several layers of chemistry on the graphene surface (Fig. 2a). Starting with the base layer of chemical vapor deposition (CVD)-grown single-layer graphene¹⁸ directly

transferred on a glass slide, we incorporated 1-pyrenebutanoic acid succinimidyl ester (pyrene-NHS) as a linker between graphene and anti-TOM20 antibody. While pyrene exhibits a strong pi-pi interaction with the graphene, NHS provides a terminal for amide bonding of antibodies. Since TOM20 is a subunit of the translocase of outer membrane, anti-TOM20 antibody can be used to attract mitochondria¹⁹. Anti-TOM20 antibodies were incubated and allowed to bond with the pyrene-NHS linker. After antibody incubation, ethanolamine was added to inactivate the NHS remaining ester bonds. Finally, TWEEN20 was added to passivate the exposed graphene area, effectively shielding the exposed graphene surface from unspecific protein adsorption.

After functionalization, the device was washed with KCl buffer (140 mM KCl, 2 mM MgCl₂, 10 mM NaCl, 0.5 mM EGTA, 0.5 mM KH₂PO₄, 2 mM HEPES, 5 mM succinate, 2 μM rotenone, pH 7.2 adjusted with KOH) twice before 40 μl of 0.14 μg/μl isolated HeLa mitochondria (0.07 μg/μl for RS4;11) was incubated in the device's chamber for 15 minutes at 4 °C. After incubation, the device was gently washed with fresh KCl buffer and then mounted on the inverted microscope. Because graphene was directly transferred on the glass slide, the focusing distance from the objective to the graphene was minimal, allowing visualization of single isolated mitochondria with fluorescence stains such as MitoTracker® Green FM. Figure 2b shows mitochondria, previously stained with MitoTracker® Green FM, are immobilized on top of the graphene layer at the bottom of the device. Gentle insertions of experimental reagents did not disturb the mitochondria as shown in Supplementary Fig. 1. In a similar fashion, a graphene device without anti-TOM20 antibody or just bare graphene was incubated with isolated mitochondria but did not result in any mitochondria attachment on the graphene surface after the wash step.

The density of mitochondria attachment was calculated to be 4237 ± 279 mitochondria/mm² for HeLa cells and $1418/\text{mm}^2 \pm 328$ for RS4;11 cells; the sample sizes were three. We used ImageJ particle analysis to count the number of mitochondria within 0.25–1 μm² under the assumption that a mitochondrion's area would fall in this range. Since the chamber's bottom area is 20 mm², we can compute that a device would have approximately 85,000 mitochondria at the upper limit. If we assumed that 1 μg of mitochondrial protein yields 10⁶ particles of isolated mitochondria²⁰, after washing, our device would require at most 0.1 μg of mitochondrial protein. This quantity is much smaller than the number of mitochondria that would be included in more conventional solution biochemistry assays, ranging from 3–20 μg mitochondrial protein for assays of cytc release²¹, single mitochondria membrane potential²², and respiration studies²³. In addition, this work pushes the minimal mitochondrial quantity requirement even further compared with our previous reports^{24,25}, which used 0.75 μg of mitochondrial protein per assay. Using our typical yield of 140 μg mitochondrial protein from 10⁷ HeLa cells, 0.1 μg of mitochondrial protein amounts to around 7000 cells worth of mitochondria, a slight improvement to the 10,000-cell requirement imposed for plate-based assays of mitochondrial functions¹⁷.

Functionalized Graphene devices are pH-sensitive, but insensitive to CCCP, BIM-BH3, and cytc, and are only mildly sensitive to succinate and K⁺ ions. We measured the depletion curves, defined as the graphene current vs. electrolyte gate voltage curve (I_{ds} vs. V_{g}), of the functionalized graphene devices with KCl buffer at different pH values. 1 M HCl and 1 M KOH were used to adjust the pH of the KCl buffer from pH 4 to 10. Figure 2c shows that the depletion curve shifts right with increasing pH, and at zero gate voltage the current increases. The gate in these experiments is the electrolyte (buffer) in the chamber. The pH sensitivity of graphene is consistent with previous reports^{26,27}. From the inset of Fig. 2c, at zero gate voltage an increase in one unit change in pH corresponds to approximately 4% increase in conductance. This calibration, however, only applies to functionalized devices without mitochondria. For the devices with tethered isolated mitochondria, the situation is more complicated and is discussed in Supplementary Fig. 3. Additionally, we carried out a series of control experiments to confirm that the dominant response of the graphene was to pH, and not other chemicals used in the buffer or likely to have been modified by the mitochondria (Fig. 2d, and Supplementary Fig. 11). Having established a relatively low sensitivity of graphene to experimental substrates (as compared to the pH sensitivity), we set out to test the graphene response in the presence of isolated mitochondria.

CCCP causes $\Delta\Psi_{\text{m}}$ to decrease and buffer pH to increase. The mitochondrial proton motive force is defined as $\Delta p = \Delta\Psi_{\text{m}} - 59\Delta\text{pH}$, where $\Delta\Psi_{\text{m}}$ denotes the mitochondrial inner membrane potential and ΔpH indicates the proton gradient across the inner membrane. The mitochondrial inner membrane potential can generally be monitored by lipophilic cations or indicator dyes. We chose 40 nM TMRE²⁸ as the membrane potential indicator. The concentration of the charged dyes (in this case, TMRE) changes with membrane potential in accordance with the Nernst equation (1), which states the concentration ratio is given by:

$$\frac{[\text{TMRE}]_{\text{in}}}{[\text{TMRE}]_{\text{out}}} = e^{-\frac{\Delta\Psi_{\text{m}}}{kT}} \quad (1)$$

This means at higher potentials (defined as the matrix is more negative), more TMRE accumulates inside the mitochondrial matrix. As a result, TMRE fluorescence intensity from inside the mitochondria can indicate qualitatively the mitochondrial membrane potential i.e. the higher the intensity, the higher the membrane potential. Assessing $\Delta\Psi_{\text{m}}$ quantitatively requires the TMRE intensity outside of the mitochondria^{16,29}, however, most studies on mitochondrial membrane potential report only the TMRE intensity inside the mitochondria^{30,31}. In addition to TMRE fluorescence, we performed concurrent electrical detection on the isolated mitochondria using graphene and correlated the electrical signal to the observed fluorescent readout. The experiments were performed in the dark with the excitation LEDs intermittently turned on to monitor TMRE fluorescence. Hence, graphene photo-conductance was minimal and no interference from the LEDs was observed from the recorded electrical signal.

Figure 3 shows the normalized change in both the graphene conductance and TMRE signal after the addition of 1 μM CCCP, a strong uncoupling agent that can abruptly depolarize the membrane potential. CCCP works as

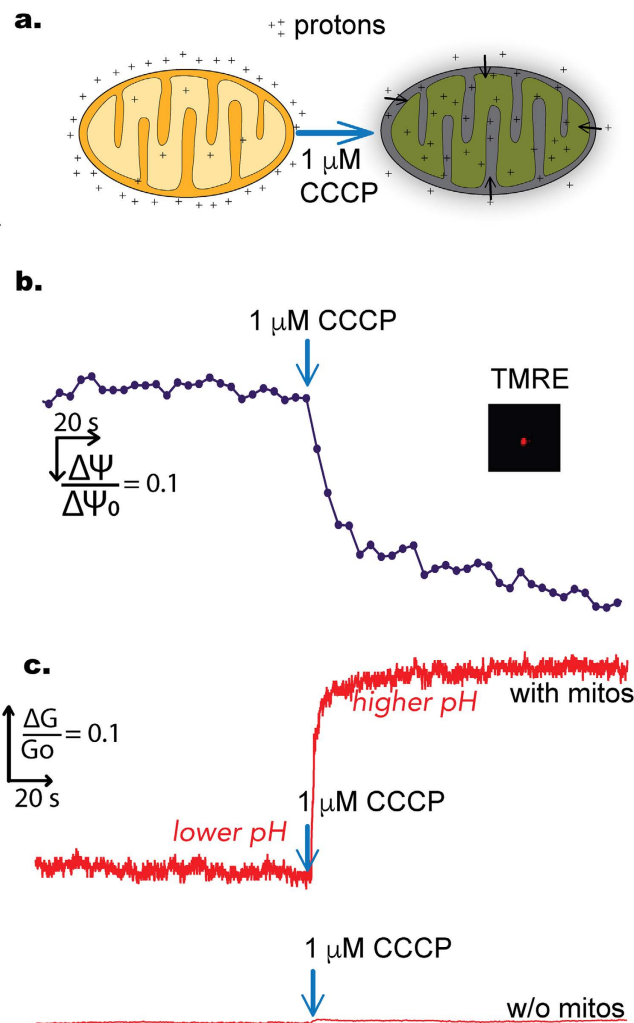


Figure 3. (a) Illustrations of protons movement after CCCP addition; (b) Time-lapse of TMRE fluorescence, an indicator of the mitochondrial membrane potential, before and after the addition of CCCP; (c) The corresponding change in graphene conductance (measured simultaneously with the fluorescence) and the control; after CCCP, the concentration of protons changes dramatically in the extra-mitochondrial buffer.

an efficient proton transfer agent that effectively short circuits the proton (pH) gradient as well as the membrane potential (charge gradient). Compared to the starting fluorescence, after addition of CCCP, the fluorescent signal, defined as TMRE intensity of one mitochondrion, dropped about fifty percent. At the same time, the graphene conductance increased by almost twenty percent, indicating a buffer pH increase.

The results for the CCCP experiment were reproduced five times yielding a statistics of increased conductance at $13 \pm 8\%$. The average reduction in TMRE intensity after CCCP addition was $69 \pm 7\%$ ($N = 3$). In addition, we also performed the same experiment but with another, albeit weaker, uncoupling agent namely $10 \mu\text{M}$ 2,4-Dinitrophenol and observed a similar change in electrical and fluorescence signals (Supplementary Fig. 4). Meanwhile, the control electrical experiments, performed on the same day with the other experiments on identically fabricated devices but without any mitochondria, yielded at most 0.8% difference in graphene conductance.

In order to confirm the alkalization of the buffer on CCCP addition, and to rule out the possibility that the graphene pH response was an artifact of the relatively novel and new graphene pH detector in the context of tethered mitochondria, we used a traditional, commercial pH meter to measure the pH change in a mitochondrial suspension. The response time of the pH meter was around 3 seconds. We diluted $200 \mu\text{g}$ isolated HeLa mitochondria in 2 mL of KCl buffer and measured the pH with an Oakton Instruments pH meter and an OrionTM ROSS pH electrode. Before CCCP, our buffer pH was 7.21 ± 0.01 which increased to 7.23 ± 0.01 after CCCP ($N = 3$). Although this measurement was right at the limit of the sensitivity of the commercial pH meter, the results were consistent with our much more sensitive graphene results.

BIM-BH3-induced MOMP causes oligomycin-independent buffer acidification ($\downarrow \text{pH}_{\text{buffer}}$) and $\Delta\psi_{\text{m}}$ decay. We utilized BIM-BH3 peptide (derived from BIM protein, see Methods for sequence) as a known activator of BAX/BAK to induce MOMP. In whole cells, BAX is soluble in the cytosol while BAK is present on the outer membrane. In our experiments, because we used isolated mitochondria where only BAK is

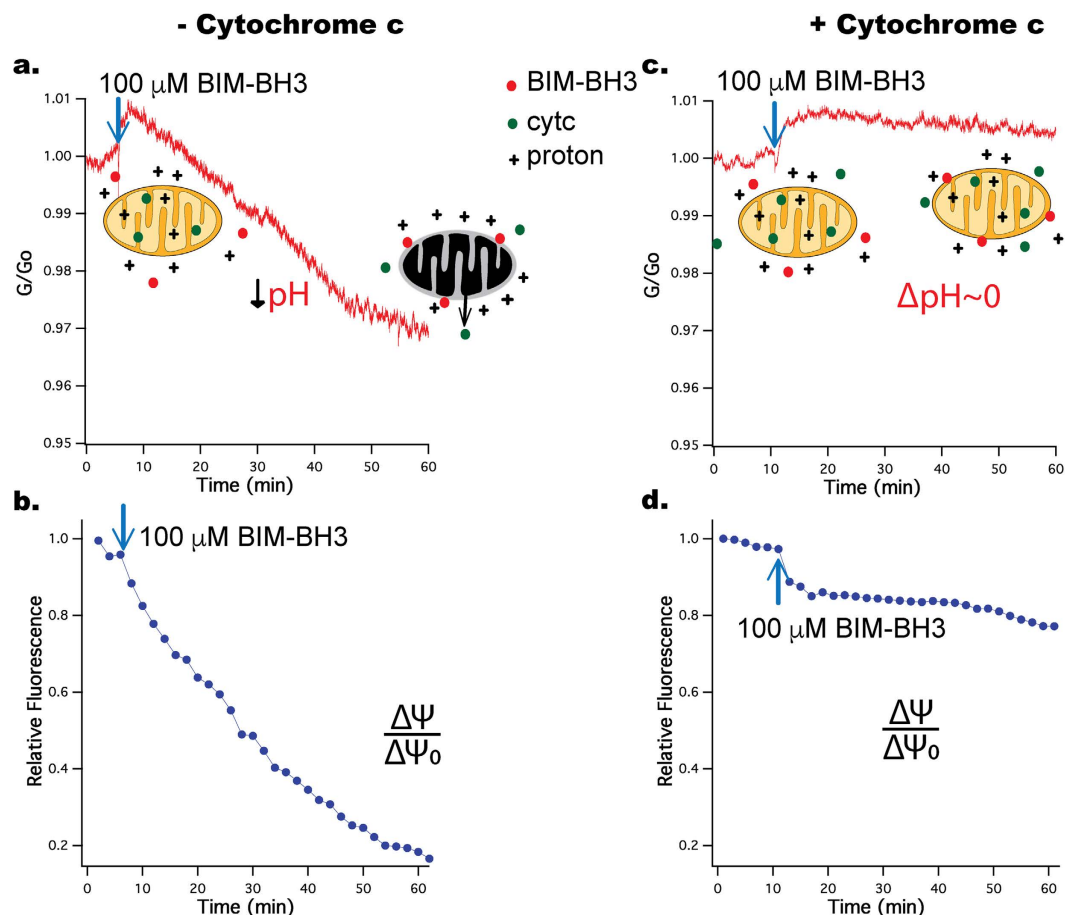


Figure 4. (a,b) Addition of 100 μ M BIM-BH3 causes graphene conductance and membrane potential to decrease. The fluorescence signal was defined as the average of three mitochondria. Results are representative of three independent experiments. (c,d) A similar experiment with 100 μ M BIM-BH3 but with 10 μ M cytc added to the buffer. The results show less reduction in both graphene conductance and membrane potential. Results are representative of two independent experiments.

present and no BAX in the buffer, BIM-BH3 could only affect BAK. Previous studies^{5,8,32} have demonstrated that BIM-BH3 can directly induce BAK homo-oligomerization, which forms pores in the mitochondrial outer membrane causing MOMP, leading to the release of cytc and other pro-death factors with a side effect being the eventual collapse of the inner membrane potential. The experiments by Letai and colleagues⁵ tested BIM-BH3 on wildtype and BAK deficient liver mitochondria and demonstrated that BIM-BH3 activates BAK oligomerization. Because BIM-BH3 can cause MOMP, one potential concern is that BIM-BH3 can disrupt the binding between the antiTOM20 antibodies and the mitochondria, thus releasing the mitochondria away from the graphene surface. This possibility is unlikely, however, since BIM-BH3 can integrate into the outer membrane without TOM20³³.

Also for the experiments with BIM-BH3, we chose RS4;11 isolated mitochondria due to their well-demonstrated outer membrane composition of BCL-2 family proteins particularly BAK³⁴. Addition of CCCP to RS4;11 mitochondria caused a comparable increase in buffer pH as seen for HeLa cell (Supplemental Fig. 5). Upon introduction of 100 μ M BIM-BH3 to the RS4;11 mitochondria, we observed a distinct acidification of the buffer (measured via decreased graphene conductance, Fig. 4a), a result confirmed with HeLa mitochondria (Supplementary Fig. 6), as well as a decline in the membrane potential (Fig. 4b). Both of these effects were observed with and without 2 μ g/ml oligomycin (which blocks the transport of protons by ATP synthase) in KCl buffer (Supplementary Fig. 8). The induced pH changes following BIM-BH3 addition occurred over a longer timescale than that resulting from CCCP exposure.

Again, as a check to confirm that the measured acidification was not an artifact of the novel graphene biosensor, we measured the buffer pH with a commercial pH meter on introduction of BIM-BH3 to a mitochondrial suspension (140 μ g of RS4;11 mitochondria in 500 μ L total volume) under otherwise identical conditions. Our measurements showed an average pH reduction of 0.05 ± 0.01 (N = 3) after 60 min of incubation with the peptide.

Exogenous cytc blocks buffer acidification and rescues $\Delta\Psi$ m after BIM-BH3 induced MOMP. During MOMP, cytc is released to the buffer so the lack of cytc results in loss of cytc mediated electron transfer between complex III and IV in the electron transport chain (ETC). This stalls the ETC, leading to a gradual decline in membrane potential and loss of respiration^{35–37}. Consistent with this hypothesis, following MOMP,

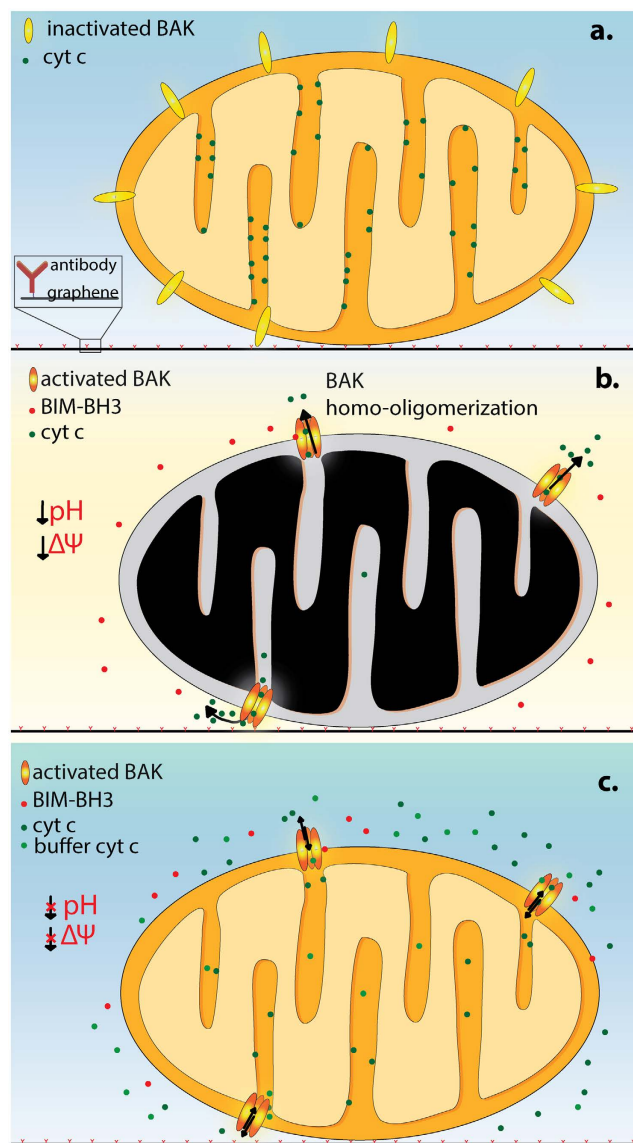


Figure 5. BIM-BH3-induced MOMP in tethered, vital, isolated mitochondria. The mitochondrion (0.5–1 μm in diameter) is drawn to scale with the antibody ($\sim 10\text{ nm}$). (a) without BIM-BH3, BAK stays inactive; (b) with BIM-BH3, BAK is activated and oligomerize to form pores in the outer membrane, causing cytc release. This is observed to result in buffer acidification and membrane potential decline; (c) With exogenous cytc in the buffer, the mitochondrion maintains inner membrane potential with a reduced change in the buffer pH.

respiration can be restored by adding exogenous cytc^{36–38}. Motivated by this observation, we decided to test the effect of exogenous cytc on buffer acidification and membrane potential in our system. The presence of cytc in the buffer does not affect the graphene sensor (Fig. 2d).

We tested the effect of including 10 μM cytc in the buffer on the graphene signal upon treating the mitochondria with 100 μM BIM-BH3 (Fig. 4c,d). The addition of exogenous cytc following BIM-BH3-induced MOMP blocks the decline of TMRE fluorescence (or $\Delta\Psi_m$) and also greatly reduces the effect of buffer acidification. To our knowledge, this inhibition of buffer acidification by exogenous cytc following MOMP is a new observation for isolated mitochondria. Separate pH measurements of mitochondrial suspensions in the presence of cytc confirm this observation, showing only 0.02 ± 0.01 reduction in buffer pH with cytc as compared to 0.05 ± 0.01 ($p < 0.05$ student t-test, $N = 3$) in the case without cytc. Figure 5 summarizes our experimental observations without any hypothesis about the mechanisms.

Discussion

We have created a novel system for assessing functional changes in mammalian mitochondria. Our system employs an optically transparent, single atom thin graphene layer onto which the mitochondria are tethered using a graphene-bound antibody against the outer membrane protein TOM20 to which isolated mitochondria adhere. Because the graphene electrode is optically transparent, single bound mitochondria can be functionally analyzed

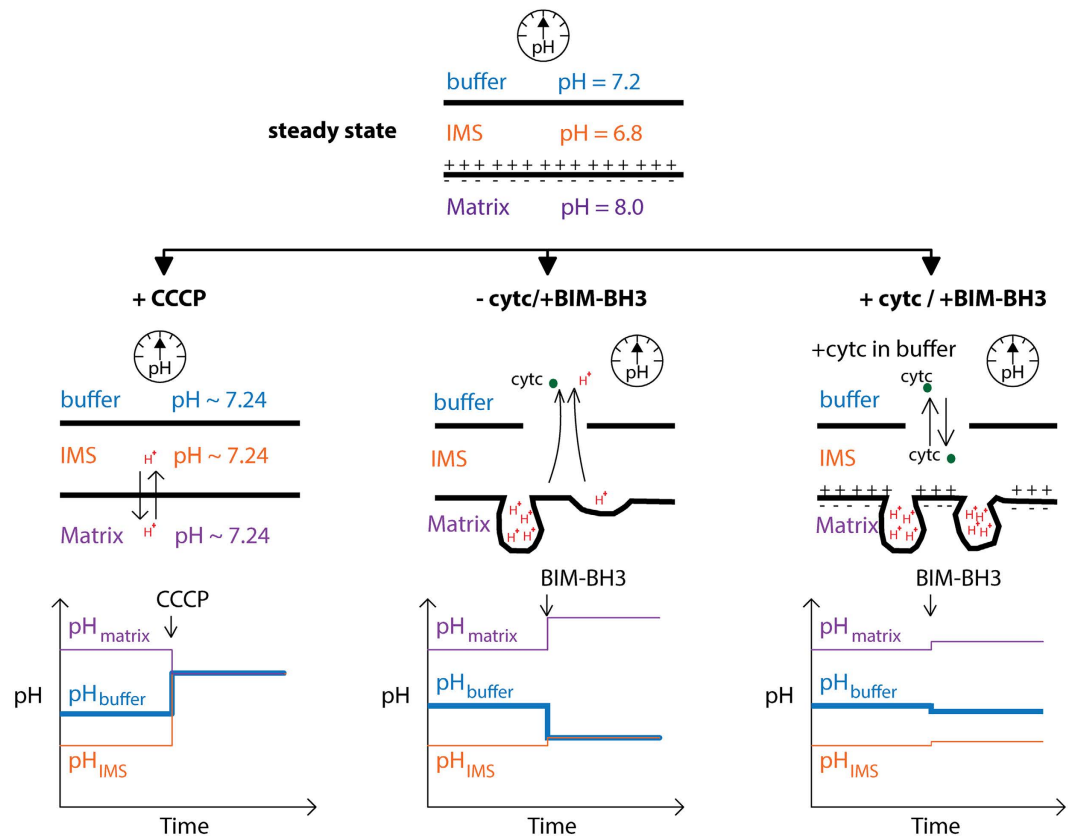


Figure 6. Schematic diagrams of membrane morphology and compartmental pHs for the three experiments performed. The steady state of the mitochondria is shown at the top with buffer pH (indicated as measured) and the other pHs as inferred from the literature^{61,62}. In the case of CCCP, pH is equilibrated across the three compartments. The bottom shows the qualitative changes in pH vs. time (not to absolute scale) with the bolded line being the measured variable while the other lines are inferred. For the next two cases, the top two figures correspond to our proposal that the cristae remodel and release protons and cytc from the invaginations and the absence of such a mechanism when exogenous cytc is added. The bottom figures indicate again the qualitative assessment of the pHs.

using analytical fluorescent dyes at the same time that the mitochondrial outer membrane can be monitored in real time by changes in the conductance of the graphene. The electrical properties of the graphene have been found to detect subtle changes in the proton concentration on the outside of the mitochondrial outer membrane as the mitochondrial inner membrane electrochemical gradient changes. The acute sensitivity of this system is permitting the dissection of alterations in the mitochondrial membrane status during various mitochondrial processes such as uncoupled depolarization of OXPHOS and the induction of the intrinsic pathway of apoptosis initiated by the pro-apoptotic peptide BIM-BH3.

Using our graphene biosensor platform, we have been able to make three important observations pertaining to the mitochondrial inner membrane electrochemical gradient and its changes during the BIM-BH3 initiated intrinsic pathway of apoptosis. First, we found that CCCP addition to respiring mitochondria causes buffer alkalinization along with membrane potential depolarization. Second, we observed that treatment of respiring mitochondria with BIM-BH3 results in external buffer acidification and membrane potential decline. Third, we found that the BIM-BH3-induced acidification and membrane potential decline of respiring mitochondria can be blocked by the addition of exogenous cytc to the external mitochondrial buffer.

Our first observation of buffer alkalinization can be attributed to CCCP allowing protons to rapidly enter the matrix. When immersed in isotonic buffer containing the mitochondrial respiratory chain complex II substrate, succinate, and the complex I inhibitor, rotenone, mitochondria rapidly oxidize the succinate passing the electrons from complex II, to coenzyme Q, to complex III, to cytc, to complex IV, and finally to O₂ to reduce it to H₂O. The flux of electrons through complex III and IV is coupled to the transport of protons from the mitochondrial matrix out across the mitochondrial inner membrane to the inter membrane space rendering the outside of the mitochondrial inner membrane acidic and positively charged and the inside negatively charged and alkaline³⁹. Addition of uncouplers to the respiring mitochondria result in the rapid flux of protons back into the mitochondrial matrix, rendering the inter-membrane space more alkaline^{40–42} (Fig. 6). Given that the mitochondrial outer membrane voltage dependent ion channel⁴³ (VDAC or porin) is freely permeable to protons this would result

in the pH of the surrounding buffer to become more alkaline, exactly as we observed, a result consistent with Mitchell's chemiosmosis theory⁴⁴ for oxidative phosphorylation (OXPHOS) coupling.

We propose that buffer acidification with BIM-BH3 in our second observation is caused by release of protons from the lumina created by the invaginations of the mitochondrial inner membrane. At first glance, the acidification of the surrounding mitochondrial buffer on treatment of respiring mitochondria with the inducer of the intrinsic pathway of apoptosis, BIM-BH3, would seem contrary to the chemiosmosis theory of OXPHOS. However, recent discoveries^{9,11,45} about structure and function of the mitochondrial inner membrane and the changes that occur during the induction of the intrinsic pathway of apoptosis render the observation of acidification explicable.

The mitochondrial inner membrane is highly invaginated and with the tips of the invaginations closest to the outer membrane held together by the mitochondrial inner membrane integral membrane protein OPA1¹⁰ located within the mitochondrial contact site and cristae organizing system (MICOS). This creates multiple internal lumina in which the interior of each lumen is equivalent to the outside of the mitochondrial inner membrane. Hence, within these lumina the cytc and proton concentration can become very high.

When the mitochondrial membrane potential declines or the intrinsic pathway of apoptosis is activated mitochondrial inner membrane proteases including OMA1 become activated and cleave OPA1 resulting in the opening of the inner membrane lumina to the mitochondrial intermembrane space^{9,11}. Since most of the cytc is encompassed within the lumina of the inner membrane^{46,47} this process is central to the release of cytc from the mitochondria observed as the intrinsic pathway of apoptosis progresses. Because protons are much smaller in diameter than cytc, it follows that as OPA1 is cleaved, the first event is the escape of the protons into the mitochondrial inter membrane space and out through the permeabilized outer membrane and into the surrounding buffer (Fig. 6). This would cause the gradual acidification of the surrounding medium detected by the graphene electrodes. Treatments of the mitochondria with BH3 peptides often require 60–90 min incubation^{17,48} before any functional measurements can detect a change. This time frame is consistent with the completion of the pH change that we detected with the graphene sensor which occurred at about 60 minutes.

Given that the decline in the mitochondrial inner membrane potential is an important prerequisite for the activation of inner membrane proteases and the cleavage of OPA1, it follows that the release of cytc from the mitochondrial inter membrane space following BIM-BH3 induced BAK activation could locally activate the proteases that cleave OPA1. This possibility follows from the conceptualization of the distribution of the respirasomes across the mitochondrial inner membrane. The respirasomes would fall into two categories: those that are located on the mitochondrial inner membranes that form the cristae invagination-generated lumina and pump protons into the cristae lumina and those respirasomes that are located in the inner membrane which faces the intermembrane space. This later set of respirasomes would be responsible for maintaining the pH acidification of the intermembrane space and thus would control the activation of the outer membrane proteases that can cleave OPA1. When BIM-BH3 activates BAK to open the outer membrane, the first cytc to be released would be that in the inter membrane space resulting in localized drop in the mitochondrial membrane potential, activating OMA1, and initiating the cleavage of OPA1. Once OPA1 is cleaved the invaginated cristae lumina would open to the inner membrane space and the remaining cytc would be released stopping all further respiration. Addition of exogenous cytc to the medium surrounding the mitochondria would sustain the respiration required for maintaining the intermembrane space pH and membrane potential thus stabilizing OPA1 and blocking detectable changes in proton and cytc release (Fig. 6), which is our third observation.

Although previous studies have shown that cytosolic acidification is associated with apoptosis in whole cells^{12,13,49}, its role, timing, and mechanism has remained until now a mystery. One proposed mechanism (ATP synthase reversal¹⁴) has been ruled out on thermodynamic grounds⁵⁰. Our observation of acidification even in the presence oligomycin (which blocks ATP synthase activity) also rules out ATP synthase involvement. Furthermore, our results provide a plausible mechanism that is consistent with recent discoveries of OMA1/OPA1 based cristae remodeling. Although it is generally believed that mitochondria remodel during apoptosis⁵¹, to directly measure cristae structure during apoptosis is technically challenging, and beyond the scope of this work. Our hypothesis that cristae remodeling causes buffer acidification is the most consistent hypothesis with our data, as well as all of the data in the literature on this subject⁵¹.

Furthermore, it is still highly plausible that the physiological role of pH change is to enhance caspase activities during apoptosis, as the caspases are known to have pH-dependent activation⁴⁹. These questions have led to a “renaissance” of interest in mitochondrial pH⁵². In addition, because the tumor microenvironment also exhibits significant pH alterations, studying mitochondrial mediated pH changes would make for fruitful future studies.

As with any new bio-assay technology, it is important to benchmark results against known standards, and to compare and contrast advantages and disadvantages of the new vs. traditional methods. For pH sensing, there are two traditional approaches: Electrochemical sensors and genetically encoded pH sensitive fluorescent proteins such as pHluorin, SypHer, and pHred. We have chosen to benchmark our results against a conventional pH meter (Oakton Instruments pH meter and an Orion™ ROSS pH electrode), and found the results to be consistent. We found this to be more expedient than engineering a separate strain with pH sensitive fluorescent proteins. However, the conventional pH meter has barely sufficient pH resolution (0.01 pH) and a slow response time, as compared to our integrated graphene detectors. Consequently, we had to use significantly more sample (140 µg vs 0.1 µg) with the pH meter, and probably because of 0.01 pH resolution we could only detect pH changes after 60 min of mitochondrial incubation with BIM-BH3. In contrast, the intimate contact between the graphene and the mitochondria allows our graphene devices to detect an estimated 4.0×10^{-4} relative change in pH unit (Supplementary Information) with 0.2 s temporal resolution. The enhanced sensitivity comes with a drawback that the pH calibration for the graphene devices is not absolute (Supplementary Information).

In principle, a genetically engineered mitochondrial pH sensor based approach has the advantage that an absolute calibration can be performed for pH sensing. However, this approach has resulted in some uncertainties

in the literature about the proton motive force dynamics during apoptosis^{14,49}. Still, recent advances in live cell imaging have enabled detailed (and calibrated) studies of mitochondrial and cytosolic pH under different metabolic conditions^{53,54}. While advantageous in many ways, genetically encoded mitochondrial pH sensors do have some disadvantages, including restricted applicability to established transformed cell lines.

What our ultrasensitive graphene system for analyzing isolated mitochondria has revealed is a model where there are two totally different mitochondrial inner membrane electrochemical gradients. One of these is the proton gradient between the mitochondria matrix and the intermembrane space. This gradient appears to be an important mediator for the regulation of OMA1 and the resulting regulation of OPA1 cleavage, the important factor in linking the opening of MOMP with the initiation of the intrinsic pathway of apoptosis. However, the second inner membrane electrochemical gradient is between the mitochondrial matrix and the enclosed lumina of the cristae invaginations which are isolated from the intermembrane space electrochemical gradient by closure of the cristae lumina by MICOs and OPA1. This structure potentially permits a much higher concentration of protons to be generated, since the pH cannot be buffered by the cytoplasm surrounding the mitochondrion. Furthermore, by confining the protons in a small volume, the electrostatic potential can be much higher increasing the energetic capacity of the system.

In conclusion, by taking advantage of our ability to study isolated mitochondria using our graphene sensor, we have been able to separate two fundamentally different classes of mitochondrial inner membrane, respirosomes, and electrochemical gradients, resulting in a strikingly new perspective of the role of the mitochondrial electrochemical gradient and thus of the biophysics associated with the Mitchell's chemiosmosis hypothesis⁴⁴.

The development of the graphene-based system for monitoring changes in the mitochondrial function permitted us to investigate events associated with mitochondrial OXPHOS coupling and the intrinsic pathway of apoptosis. However, we have only begun to monopolize on the exquisite time and sensitivity resolution that our new system permits. Further miniaturization of the technology from millimeter to micrometer dimensions (a straightforward process using photolithography) could enable assays on single mitochondria. In addition to the studies presented herein, this platform could enable new studies of mitochondrial biology and medicine that were heretofore inaccessible. The first possibility is the parallelization from one to thousands of on-chip devices. Such a system could permit for the first time the analysis of 1) mitochondrial heterogeneity within a single cell, say as mtDNA mutations in heteroplasmy⁵⁵ leading to functional heterogeneity, an unexplored frontier in mitochondrial biology; 2) massively parallel screening for peptides and drugs that could modulate mitochondrial respiration or the intrinsic pathway of apoptosis. For example, it has recently been shown that mitochondrial sensitivity to apoptosis/MOMP/cytc release in response to chemotherapies in tumor biopsies (*in vitro*) is directly correlated with patient survival rate⁵⁶. Further investigation has led to a proposed "profile" of each tumor, defined as its qualitative response (defined as cytc release) to a panel of peptides, entitled "BH3 profiling"¹⁷. Another potential application is high temporal resolution, high pH resolution studies of mitochondrial flashes^{54,57}. The role of these flashes, and their relationship to signaling pathways, metabolism, bioenergetics, apoptosis and the mitochondrial permeability transition pore is only now beginning to be understood.

Methods

Graphene transfer and device fabrication. Graphene was transferred on to glass substrates using a modified protocol from what we described previously¹⁸. Briefly, a 5 cm × 5 cm copper foil containing CVD grown single-layer graphene on one side was cut into 0.6 cm × 1.0 cm sheets. The side of the sheet containing graphene was pressed lightly against a block of pre-cured PDMS. The Cu-graphene-PDMS structure was then placed and left floating in a Cu-etchant bath (50 mg/ml ammonium persulfate in DI water). After the copper was completely etched away, the graphene-PDMS structure was washed three times with DI H₂O for one hour to eliminate any residual ions from the copper etching step. The wet PDMS/graphene block was then pressed against a 1-mm thick glass slide that had been cleaned for one hour with 1:3 (v/v) H₂O₂:H₂SO₄ solution. The glass-graphene-PDMS slide was kept under a slight pressure overnight to promote graphene-glass adhesion and allow the interfacial water to evaporate. When the device was completely dry, the PDMS was carefully peeled off, leaving large-area single-layer graphene on the glass slide. Although many transfer steps were essentially similar to the protocol¹⁸, the deposition of graphene directly on glass was the modification in the study.

Following graphene transfer, we needed to create an experimental chamber on top of the graphene, fabricate drain and source electrodes to measure the graphene in-plane conductance, and insulate the electrodes from the experimental liquid. To accomplish these goals, a simple, freshly cured PDMS slab with an inner cut-out was placed directly on top of the graphene (Fig. 2b). Specifically, the cutout, measured 4 mm × 5 mm × 3 mm in length × width × height, serves as the experimental chamber. Additionally, due to having narrow width, the PDMS slab, although covering most graphene area, still leaves some exposed graphene where quick-dry silver paste (Ted Pella) can be painted to establish electrical connection. As depicted in Fig. 2b, the silver paste electrodes are conveniently insulated from the experimental chamber.

Graphene functionalization. After the silver-paste electrodes were completely dry, graphene functionalization was carried out using a series of solution deposition, incubation and wash. Each step in the series employed 50 μL volume. First, 3.81 mg of pyrene-NHS was mixed with 2 mL dimethylformamide (DMF), and added to the PDMS chamber of each graphene device. Incubation with pyrene-NHS ensued for one hour at room temperature. The device was then washed sequentially with fresh DMF, DI water and PBS pH 7.2. Anti-TOM20 antibody (Santa Cruz Biotechnology) solution is added at 33.3 μg/mL concentration and incubated overnight at 4 °C. After two wash steps with PBS then DI H₂O, 0.1 M ethanolamine diluted in DI H₂O was added and incubated for one hour at room temperature then washed with DI H₂O. The next incubation with 0.1% TWEEN-20 was set for one hour at room temperature to deactivate the exposed graphene area by preventing unspecific protein adsorption.

The functionalization scheme was partially adapted from⁵⁸. Finally, the devices were washed with DI H₂O then KCl buffer for immediate use.

While the fabrication and functionalization steps might at first seem straightforward, our device yield was around fifty percent. The limiting factor here was the bonding strength between the final PDMS and glass slide, which often resulted in leakage at the DMF step or the overnight incubation at 4 °C. DMF is an organic solvent, which might affect the integrity of PDMS; hence, we remedied by taking extreme care not to spill the solvent anywhere outside of the chamber. Furthermore, we attributed the failing rate at 4 °C step to the humidity inside the refrigerator, so putting the device in a desiccator did increase our yield. We consider fifty percent yield was reasonably robust for our experiments because we would have at least three working (with electrical connections and no liquid leakage) devices on the days of the experiment.

Cell culture and mitochondria isolation. *Cell Preparation.* The mammalian cell lines: HeLa and RS4;11 (American Type Culture Collection) were maintained in the log growth phase using the appropriate tissue culture protocols for adherent and suspension cells, respectively. All cell culture related supplies such as media, fetal bovine serum, PBS pH 7.2, mitochondria staining dyes and trypsin were obtained from Life Technologies. On the days of the experiment, 10⁷ cells were typically harvested for mitochondria isolation. We used more cells if we needed more mitochondria.

Mitochondria Staining. Before isolation, the confluent cells were stained with 100 nM MitoTracker® Green FM and 40 nM TMRE for 1 hour. Subsequent isolation steps used solutions with 40 nM TMRE because TMRE is a potentiometric dye, which fluctuates in and out of the mitochondria depending on their inner membrane potential. 40 nM was determined as the optimal concentration for our experiments (Supplementary Fig. 7).

Mitochondria Isolation. Our complete isolation buffer contains 225 mM mannitol, 75 mM sucrose, 0.5 mM EGTA, 20 mM HEPES, 0.5% (w/v) BSA, 1X protease inhibitor, pH 7.2 with 1 M KOH. All chemicals were purchased from Sigma Aldrich. The stock isolation buffer was prepared without BSA and the protease inhibitor and stored at 4 °C. Mitochondria from the cultured cells were isolated using differential centrifugation. After collection, the cells were transferred to a glass homogenization tube in 3 mL of complete isolation buffer and homogenized with 30 strokes on ice for HeLa cells and 40 strokes for RS4;11. The cells were then transferred into 2-ml Eppendorf tubes and centrifuged at a low speed of 2000xg for 4 min at 4 °C. The resulting supernatant was collected and centrifuged at a high speed of 12,000xg × 10 min at 4 °C. After this step, the supernatant as well as the light-colored fluffy sediment containing damaged mitochondria were aspirated and the resulting pellet was resuspended in KCl buffer (140 mM KCl, 2 mM MgCl₂, 10 mM NaCl, 0.5 mM EGTA, 0.5 mM KH₂PO₄, 2 mM HEPES, 5 mM succinate, 2 μM rotenone, pH 7.2 adjusted with KOH). However, for mitochondria protein analysis, the mitochondria were resuspended in KCl buffer without EGTA. The protein analysis was done with BCA assay kit supplied by Thermo Fisher Scientific. A typical mitochondrial preparation with this protocol exhibits a respiratory control ratio of 3.1 (measured with a Hansatech Oxytherm), which is good for cultured cells⁵⁹.

Fluorescence measurement. Using an Olympus IX71 inverted microscope with two LED excitation sources (490 nm & 565 nm), we observed the red and green fluorescence signals from MitoTracker® Green FM and TMRE. Our field of view from our 20X objective is 200 μm × 300 μm, and we monitored the fluorescence from this field of view by controlling the microscope with NIH Micromanager software, which also set the exposure time to one second.

To process and analyze the images, ImageJ software was used. For the entire field of view analysis, we measured the fluorescence intensity from the field of view. In contrast, for single mitochondrion analysis, we defined regions of interest enclosing the mitochondria and three more identical copies of that region of interest to define the background noise. We then assigned the fluorescence signal of the mitochondria as the measured signal subtracting the noise average.

Experimental design and electrical measurement. After mitochondria isolation, we loaded about 6 μg of mitochondrial protein of isolated mitochondria to a graphene device and incubated the device for 15 min at room temperature. Following two gentle washes with KCl buffer, the device was secured on the microscope stage, and the focus was adjusted. We then attached electrical contacts to the drain and source terminals of the devices using nickel (type) probes. The gate electrode was a Ag/AgCl electrode. An Agilent sourcemeter B2902A was used to apply the drain-source and gate voltages and to measure the currents. When both optical focus and electrical connection were satisfactory, we proceeded with taking MitoTracker® Green FM images and I_{ds} versus V_g curve, and then started both the electrical measurement of I_{ds} versus time and the fluorescence time-lapse measurement of TMRE signal. The electrical data sampling rate was 200 ms/point. In contrast, fluorescence images were taken once every 5 s for the experiments with CCCP or every 2 min for the experiments with BIM-BH3.

The starting volume of our chamber was 45 μL. During the experiment, we added 4.5 μL of the appropriate experimental substrate to achieve its final concentration. Extreme care was taken not to disturb the gate electrode. CCCP and cytc were obtained from Sigma Aldrich. BIM-BH3 peptide (sequence: MRPEIWI AQELRRIGDEFNA) was purchased from Synpeptide with a confirmation of >95% purity.

Control experiments were carried out in a similar manner with the only difference being the lack of isolated mitochondria. IGOR software was used to analyze all electrical data and the fluorescence data that were exported from ImageJ software.

Our KCl buffer contains 5 mM succinate as a carbon source for the mitochondria, facilitating the maintenance of ΔΨ_m. Since the electrons derived from succinate doesn't go through complex I, we also added rotenone. Our choice of succinate and rotenone aimed to limit ROS production by complex I⁶⁰. We also intentionally left out

ADP in our respiration buffer to avoid ATP synthase activation. In other words, we maximized $\Delta\Psi_m$, maintaining a functional but not functioning ETC, and also limiting ROS production by complex I.

References

- Wallace, D. C. Mitochondria and cancer. *Nat. Rev. Cancer* **12**, 685–698 (2012).
- Sarosiek, K. A., Chonghaile, T. N. & Letai, A. Mitochondria: gatekeepers of response to chemotherapy. *Trends Cell Biol.* **23**, 612–619 (2013).
- Rustin, P. & Kroemer, G. Mitochondria and cancer. *Ernst Shering Found. Symp. Proc.* **4**, 1–21 (2008).
- Peixoto, P. M. *et al.* MAC inhibitors antagonize the pro-apoptotic effects of tBid and disassemble Bax/Bak oligomers. *J. Bioenerg. Biomembr.* doi: 10.1007/s10863-015-9635-7 (2015).
- Letai, A. *et al.* Distinct BH3 domains either sensitize or activate mitochondrial apoptosis, serving as prototype cancer therapeutics. *Cancer Cell* **2**, 183–192 (2002).
- Kluck, R. M., Bossy-Wetzel, E., Green, D. R. & Newmeyer, D. D. The release of cytochrome c from mitochondria: a primary site for Bcl-2 regulation of apoptosis. *Science* **275**, 1132 (1997).
- Kroemer, G., Galluzzi, L. & Brenner, C. Mitochondrial membrane permeabilization in cell death. *Physiol. Rev.* **87**, 99–163 (2007).
- Chipuk, J. E., Moldoveanu, T., Llambi, F., Parsons, M. J. & Green, D. R. The BCL-2 family reunion. *Mol. Cell* **37**, 299–310 (2010).
- Jiang, X., Jiang, H., Shen, Z. & Wang, X. Activation of mitochondrial protease OMA1 by Bax and Bak promotes cytochrome c release during apoptosis. *Proc. Natl. Acad. Sci. USA* **111**, 14782–14787 (2014).
- Frezza, C. *et al.* OPA1 controls apoptotic cristae remodeling independently from mitochondrial fusion. *Cell* **126**, 177–189 (2006).
- Head, B., Griparic, L., Amiri, M., Gandre-Babbe, S. & van der Blik, A. M. Inducible proteolytic inactivation of OPA1 mediated by the OMA1 protease in mammalian cells. *J. Cell Biol.* **187**, 959–966 (2009).
- Gottlieb, R. A., Nordberg, J., Skowronski, E. & Babior, B. M. Apoptosis induced in Jurkat cells by several agents is preceded by intracellular acidification. *Proc. Natl. Acad. Sci. USA* **93**, 654–658 (1996).
- Khaled, A. R., Kim, K., Hofmeister, R., Muegge, K. & Durum, S. K. Withdrawal of IL-7 induces Bax translocation from cytosol to mitochondria through a rise in intracellular pH. *Proc. Natl. Acad. Sci. USA* **96**, 14476–14481 (1999).
- Matsuyama, S., Llopis, J., Deveraux, Q. L., Tsien, R. Y. & Reed, J. C. Changes in intramitochondrial and cytosolic pH: early events that modulate caspase activation during apoptosis. *Nat. Cell Biol.* **2**, 318–325 (2000).
- Brand, M. D. & Nicholls, D. G. Assessing mitochondrial dysfunction in cells. *Biochem. J.* **435**, 297–312 (2011).
- Nicholls, D. G. Fluorescence measurement of mitochondrial membrane potential changes in cultured cells. *Methods* **810**, 119–133 (2012).
- Ryan, J. & Letai, A. BH3 profiling in whole cells by fluorimeter or FACS. *Methods* **61**, 156–164 (2013).
- Wang, Y. Y. & Burke, P. J. A large-area and contamination-free graphene transistor for liquid-gated sensing applications. *Appl. Phys. Lett.* **103**, 52103 (2013).
- Kayo, S., Bahnemann, J., Klauser, M., Pörtner, R. & Zeng, A.-P. A microfluidic device for immuno-affinity-based separation of mitochondria from cell culture. *Lab Chip* **13**, 4467–4475 (2013).
- Gear, A. R. & Bednarek, J. M. Direct counting and sizing of mitochondria in solution. *J. Cell Biol.* **54**, 325–345 (1972).
- Ryan, J., Brunelle, J. K. & Letai, A. Heightened mitochondrial priming is the basis for apoptotic hypersensitivity of CD4+ CD8+ thymocytes. *Proc. Natl. Acad. Sci.* **107**, 12895–12900 (2010).
- Vergun, O., Votyakova, T. V. & Reynolds, I. J. Spontaneous changes in mitochondrial membrane potential in single isolated brain mitochondria. *Biophys. J.* **85**, 3358–3366 (2003).
- Rogers, G. W. *et al.* High throughput microplate respiratory measurements using minimal quantities of isolated mitochondria. *PLoS One* **6**, e21746 (2011).
- Lim, T.-S., Davila, A., Wallace, D. C. & Burke, P. J. Assessment of mitochondrial membrane potential using an on-chip microelectrode in a microfluidic Device. *Lab Chip* **10**, 1683–1688 (2010).
- Lim, T.-S., Davila, A., Zand, K., Wallace, D. C. & Burke, P. J. Wafer-scale mitochondrial membrane potential assays. *Lab Chip* **12**, 2719–2725 (2012).
- Ohno, Y., Maehashi, K., Yamashiro, Y. & Matsumoto, K. Electrolyte-gated graphene field-effect transistors for detecting pH and protein adsorption. *Nano Lett.* **9**, 3318–3322 (2009).
- Wang, Y. Y. & Burke, P. J. Polyelectrolyte multilayer electrostatic gating of graphene field-effect transistors. *Nano Res.* **7**, 1650–1658 (2014).
- Scaduto, R. C. & Grotyohann, L. W. Measurement of mitochondrial membrane potential using fluorescent rhodamine derivatives. *Biophys. J.* **76**, 469–477 (1999).
- Gerencser, A. A. *et al.* Quantitative measurement of mitochondrial membrane potential in cultured cells: calcium-induced de- and hyperpolarization of neuronal mitochondria. *J. Physiol.* **590**, 2845–2871 (2012).
- Huser, J. & Blatter, L. A. Fluctuations in mitochondrial membrane potential caused by repetitive gating of the permeability transition pore. *Biochem. J.* **343**, 311–317 (1999).
- Collins, T. J., Berridge, M. J., Lipp, P. & Bootman, M. D. Mitochondria are morphologically and functionally heterogeneous within cells. *EMBO J.* **21**, 1616–1627 (2002).
- Ren, D. *et al.* BID, BIM, and PUMA are essential for activation of the BAX- and BAK-dependent cell death program. *Science* **330**, 1390–1393 (2010).
- Frank, D. O. *et al.* The pro-apoptotic BH3-only protein Bim interacts with components of the translocase of the outer mitochondrial membrane (TOM). *PLoS One* **10**, e0123341 (2015).
- Del, V. *et al.* BCL-2 dependence and ABT-737 sensitivity in acute lymphoblastic leukemia BCL-2 dependence and ABT-737 sensitivity in acute lymphoblastic leukemia. *Leukemia* **111**, 2300–2309 (2008).
- Ow, Y. P., Green, D. R., Hao, Z. & Mak, T. W. Cytochrome c: functions beyond respiration. *Nat. Rev. Mol. Cell Biol.* **9**, 532–542 (2008).
- Mootha, V. K. *et al.* A reversible component of mitochondrial respiratory dysfunction in apoptosis can be rescued by exogenous cytochrome c. *EMBO J.* **20**, 661–671 (2001).
- Waterhouse, N. J. *et al.* Cytochrome c maintains mitochondrial transmembrane potential and ATP generation after outer mitochondrial membrane permeabilization during the apoptotic process. *J. Cell Biol.* **153**, 319–328 (2001).
- Giordano, A. *et al.* tBid induces alterations of mitochondrial fatty acid oxidation flux by malonyl-CoA-independent inhibition of carnitine palmitoyltransferase-1. *Cell Death Differ.* **12**, 603–613 (2005).
- Nicholls, D. & Ferguson, S. *Bioenergetics*. Elsevier (2013).
- Heytler, P. G. Uncoupling of oxidative phosphorylation on carbonyl cyanide phenylhydrazones. *Biochemistry* **2**, 357–361 (1963).
- Kasianowicz, J., Benz, R. & McLaughlin, S. The kinetic mechanism by which CCCP (carbonyl cyanide m-Chlorophenylhydrazone) transports protons across membranes. *J. Membr. Biol.* **82**, 179–190 (1984).
- Hirose, S., Yaginuma, N. & Inada, Y. Disruption of charge separation followed by that of the proton gradient in the mitochondrial membrane by CCCP. *J. Biochem.* **76**, 213–216 (1974).
- McCommis, K. S. & Baines, C. P. The role of VDAC in cell death: friend or foe? *Biochim. Biophys. Acta* **1818**, 1444–1450 (2012).
- Mitchell, P. Coupling of phosphorylation to electron and hydrogen transfer by a chemi-osmotic type of mechanism. *Nature* **191**, 144–148 (1961).

45. Kim, T.-H. *et al.* Bid–cardiolipin interaction at mitochondrial contact site contributes to mitochondrial cristae reorganization and cytochrome c release. *Mol. Biol. Cell* **15**, 3061–3072 (2004).
46. Perotti, E., Anderson, W. & Swift, H. Quantitative cytochemistry of the diaminobenzidine cytochrome oxidase reaction product in mitochondria of cardiac muscle and pancreas. *J. Histochem. Cytochem.* **31**, 351–365 (1985).
47. Scorrano, L. *et al.* A distinct pathway remodels mitochondrial cristae and mobilizes cytochrome c during apoptosis. *Dev. Cell* **2**, 55–67 (2002).
48. Renault, T. T., Floros, K. V. & Chipuk, J. E. BAK/BAX activation and cytochrome c release assays using isolated mitochondria. *Methods* **61**, 146–155 (2013).
49. Park, H. J., Lyons, J. C., Ohtsubo, T. & Song, C. W. Acidic environment causes apoptosis by increasing caspase activity. *Br. J. Cancer* **80**, 1892–1897 (1999).
50. Nicholls, D. G. *et al.* Apoptosis and the laws of thermodynamics. *Nat. Cell Biol.* **2**, E172 (2000).
51. Perkins, G. A. & Ellisman, M. H. In *Mitochondria and Cell Death* (ed. Hockenbery, D.) 85–110 (Humana Press, 2016), doi: 10.1007/978-1-4939-3612-0.
52. Santo-Domingo, J. & Demaurex, N. The renaissance of mitochondrial pH. *J. Gen. Physiol.* **139**, 391–393 (2012).
53. Poburko, D., Santo-domingo, J. & Demaurex, N. Dynamic Regulation of the Mitochondrial Proton Gradient during Cytosolic Calcium Elevations. *J. Biol. Chem.* **286**, 11672–11684 (2011).
54. Santo-Domingo, J., Giacomello, M., Poburko, D., Scorrano, L. & Demaurex, N. OPA1 promotes pH flashes that spread between contiguous mitochondria without matrix protein exchange. *EMBO J.* **32**, 1927–1940 (2013).
55. Payne, B. A. I. *et al.* Universal heteroplasmy of human mitochondrial DNA. *Hum. Mol. Genet.* **22**, 384–390 (2013).
56. Ni Chonghaile, T. *et al.* Pretreatment mitochondrial priming correlates with clinical response to cytotoxic chemotherapy. *Science* **334**, 1129–1133 (2011).
57. Wang, X. *et al.* Protons trigger mitochondrial flashes. *Biophys. J.* **111**, 386–394 (2016).
58. Huang, Y., Dong, X., Liu, Y., Li, L.-J. & Chen, P. Graphene-based biosensors for detection of bacteria and their metabolic activities. *J. Mater. Chem.* **21**, 12358 (2011).
59. Frezza, C., Cipolat, S. & Scorrano, L. Organelle isolation: functional mitochondria from mouse liver, muscle and cultured fibroblasts. *Nat. Protoc.* **2**, 287–295 (2007).
60. Brand, M. D. The sites and topology of mitochondrial superoxide production. *Exp. Gerontol.* **45**, 466–472 (2010).
61. Cortese, J. D., Voglino, A. L. & Hackenbrock, C. R. The ionic strength of the intermembrane space of intact mitochondria is not affected by the pH or volume of the intermembrane space. *Biochim. Biophys. Acta* **1100**, 189–197 (1992).
62. Porcelli, A. M. *et al.* pH difference across the outer mitochondrial membrane measured with a green fluorescent protein mutant. *Biochem. Biophys. Res. Commun.* **326**, 799–804 (2005).

Acknowledgements

This work was supported in part by the following grants awarded to D.C.W.: NIH RO1NS21328, RO1OD010944. P.B. acknowledges support of this work from a joint grant with D.C.W. and A.G.L. NIH IMAT R33CA183384, as well as support from the ARO (MURI W911NF-11-1-0024). Ted Pham is supported by the National Science Foundation Lifechips Integrative Graduate Education and Research Traineeship 0 549 479. We thank Jenny Lee for assistance in mitochondria isolation.

Author Contributions

T.D.P., P.J.B. and A.G.L. designed the experiments; T.D.P. performed the experiments. T.D.P. and P.J.B. wrote the manuscript; T.D.P., A.G.L., D.C.W. and P.J.B. revised the manuscript, P.Q.P. provided graphene, J.L. helped with instrumentation.

Additional Information

Supplementary information accompanies this paper at <http://www.nature.com/srep>

Competing financial interests: The authors declare no competing financial interests.

How to cite this article: Pham, T. D. *et al.* Cristae remodeling causes acidification detected by integrated graphene sensor during mitochondrial outer membrane permeabilization. *Sci. Rep.* **6**, 35907; doi: 10.1038/srep35907 (2016).

Publisher's note: Springer Nature remains neutral with regard to jurisdictional claims in published maps and institutional affiliations.



This work is licensed under a Creative Commons Attribution 4.0 International License. The images or other third party material in this article are included in the article's Creative Commons license, unless indicated otherwise in the credit line; if the material is not included under the Creative Commons license, users will need to obtain permission from the license holder to reproduce the material. To view a copy of this license, visit <http://creativecommons.org/licenses/by/4.0/>

© The Author(s) 2016

SUPPLEMENTARY INFORMATION

Cristae remodeling causes acidification detected by integrated graphene sensor during mitochondrial outer membrane permeabilization

Ted D. Pham¹, Phi Q. Pham², Jinfeng Li², Anthony G. Letai³, Douglas C. Wallace⁴, Peter J. Burke^{1,2,5}

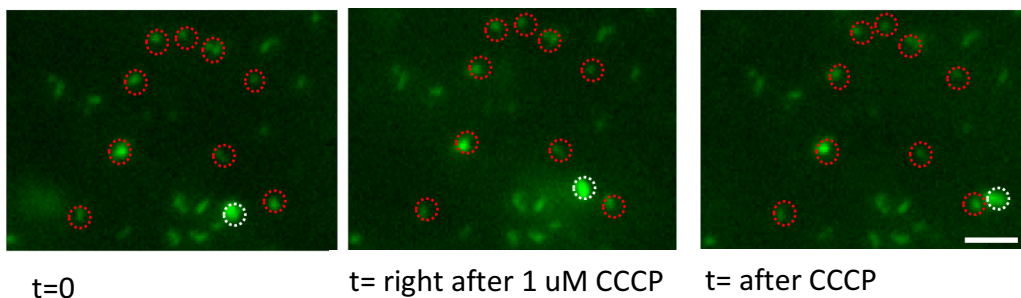
¹Department of Biomedical Engineering, University of California, Irvine, CA, USA

²Department of Chemical Engineering and Materials Science, University of California, Irvine, CA, USA

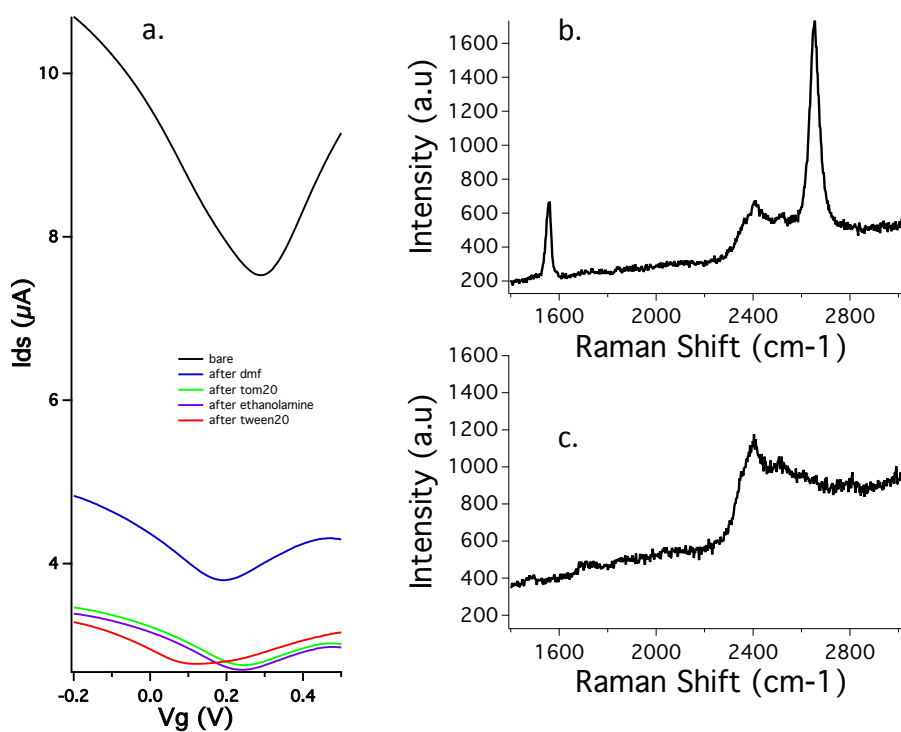
³Dana-Farber Cancer Institute, Harvard University, Boston, MA, USA

⁴Center for Mitochondrial and Epigenomic Medicine, Children's Hospital of Philadelphia and Department of Pathology and Laboratory Medicine, University of Pennsylvania, Philadelphia, PA, USA

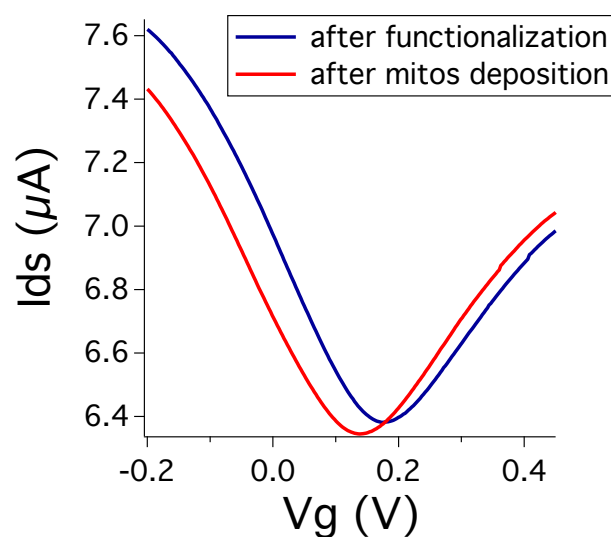
⁵Department of Electrical Engineering and Computer Science, University of California, Irvine, CA, USA
Correspondence should be addressed to P.J.B. (email:pburke@uci.edu)



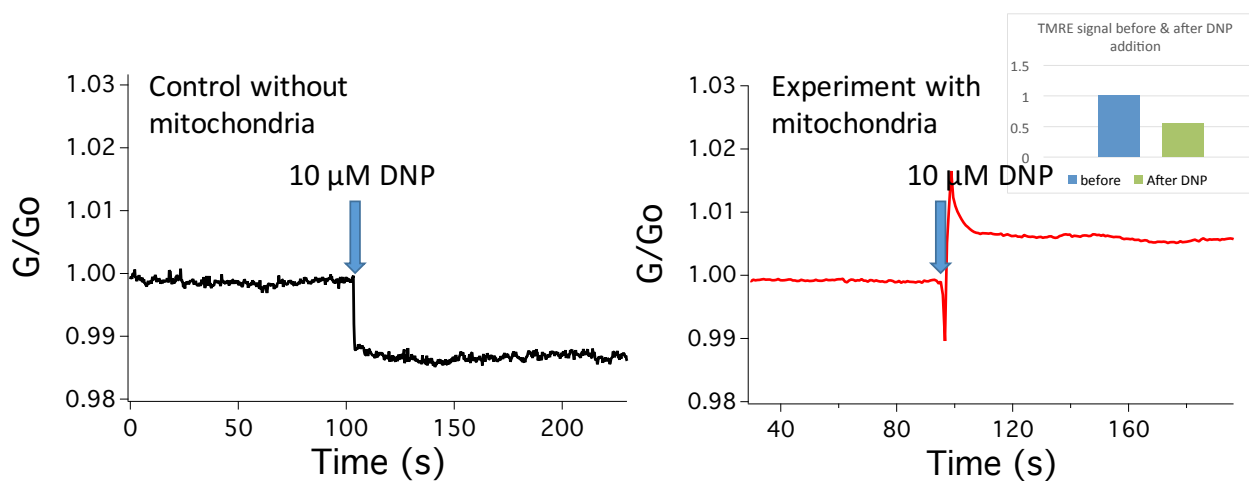
Supplementary Figure 1: Mitochondria, stained with MitoTracker→ Green FM, on graphene. Red circles indicate some immobilized mitochondria; the white circle denotes one mitochondrion moving during the experiment. Unattached mitochondria are thus considered negligible. MitoTracker→ Green FM is not potential sensitive. Scale bar is 5 μm .



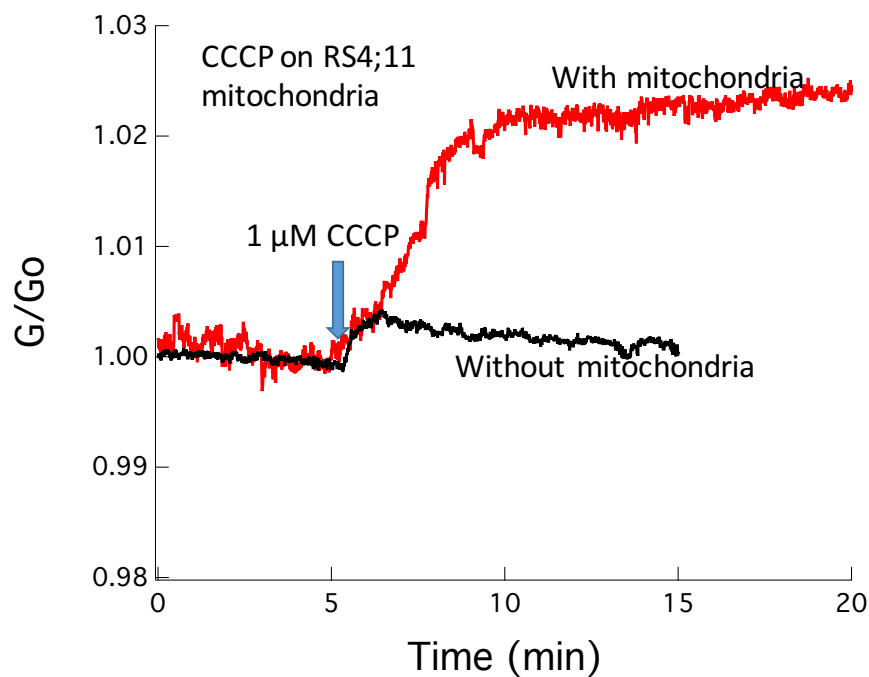
Supplementary Figure 2: (a) Graphene characterization after each functionalization step; (b) Raman spectrum confirms single-layer graphene; (c) Raman spectrum of the glass substrate explains the irregular peak around 2400 $1/\text{cm}$ in (b)



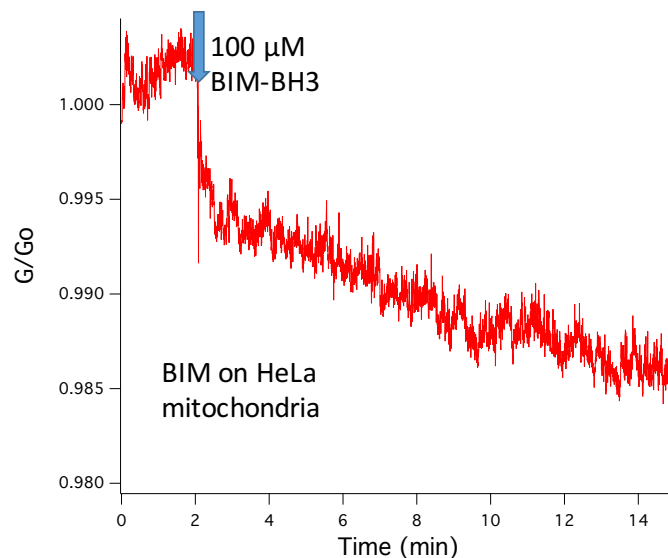
Supplementary Figure 3: Mitochondria deposition shifts the depletion curve. This effect prevents the absolute calibration of pH and renders the calibration on functionalized devices without mitochondria inapplicable to calculating the exact pH change. In addition, exposing the mitochondria to different pH solutions for calibration would adversely affect the mitochondrial functions. Results representative of four experiments.



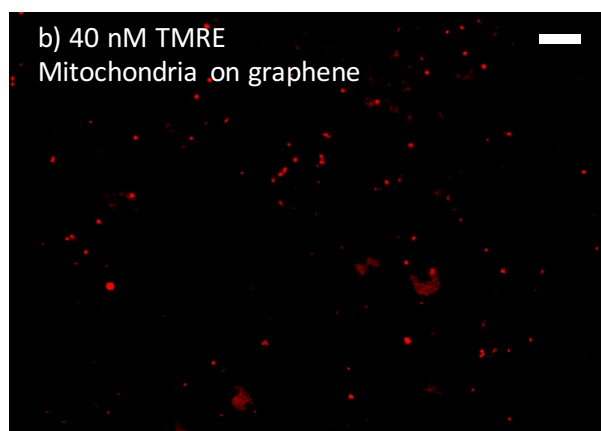
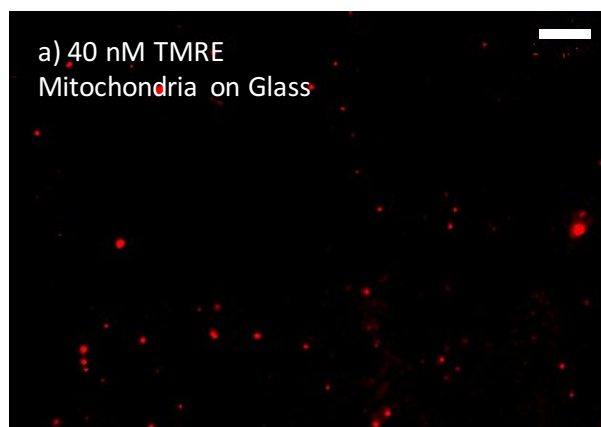
Supplementary Figure 4: Adding 10 μM 2,4-Dinitrophenol (DNP) causes the graphene conductance to increase (Red curve). This effect is expected because DNP is an uncoupling agent similar to CCCP. The inset shows the corresponding loss of membrane potential through TMRE signal. Without mitochondria, however, DNP reduces the conductance by one percent. We think this reduction is due to DNP's low pK_a of 4.114. This experiment was done once. HeLa cells were used.



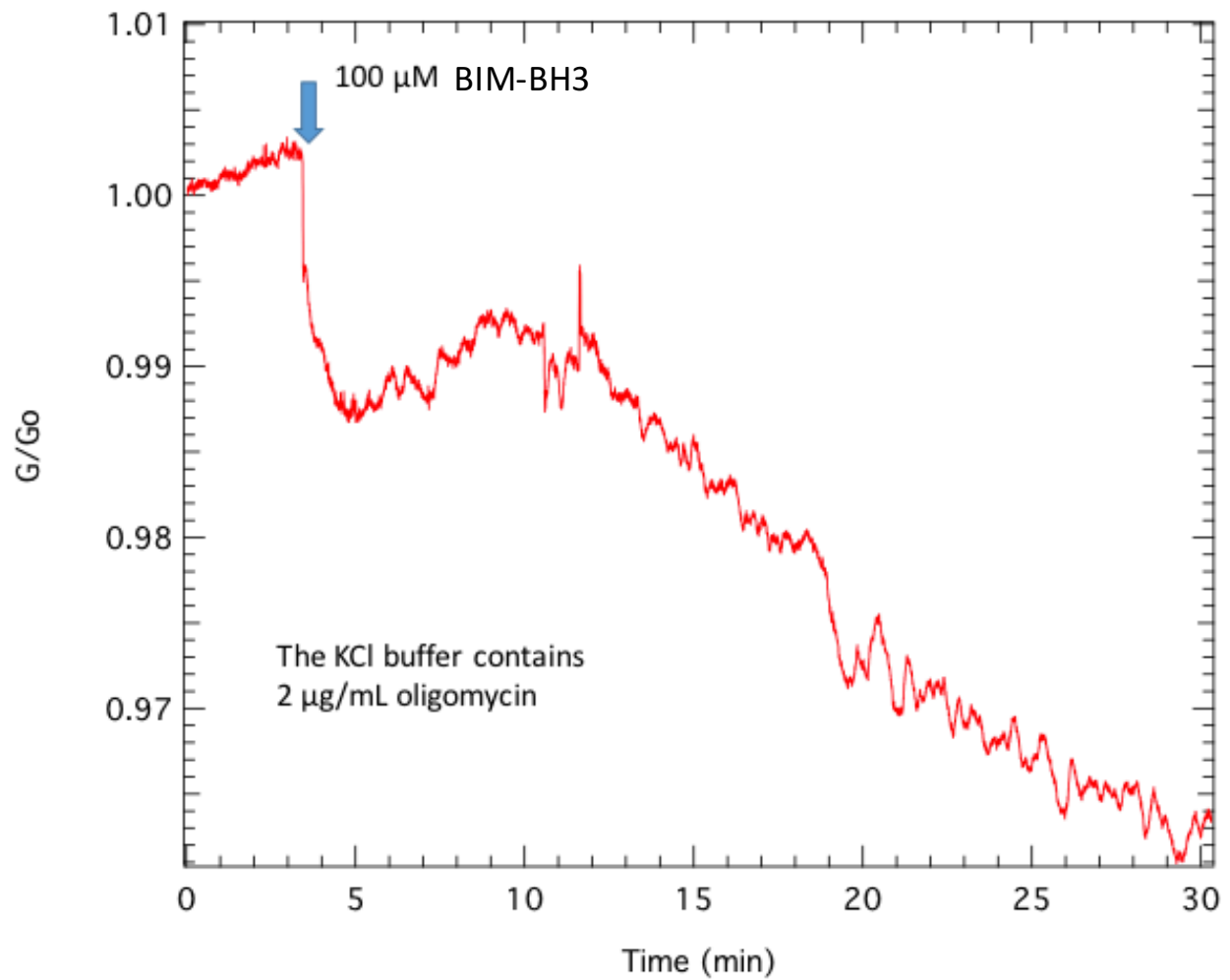
Supplementary Figure 5: Adding 1 μ M of CCCP to isolated RS4;11 mitochondria causes the graphene conductance to increase. The increase is relatively smaller than in the case of HeLa mitochondria. This is probably due to the lower quantity of mitochondria obtained from RS4;11. This experiment was done once.



Supplementary Figure 6: Adding BIM to isolated HeLa mitochondria also causes a gradual decrease in the graphene conductance. This experiment was done once. The buffer also contains 2 μ g/mL oligomycin.



Supplementary Figure 7: We compare 40 nM TMRE stained mitochondria on glass a) and on graphene b); scale bars are 10 μm , false colored red in ImageJ. The contrast level was adjusted to show mitochondria are clearly visible above the background. The signal to noise ratios in both cases are comparable.



Supplementary Figure 8: Inclusion of 2 μ g/mL oligomycin (which blocks ATP synthase) in the KCl buffer does not affect acidification. Mitochondria were isolated from RS4;11 cells. This experiment was done once. Similar results are shown in Supplementary Figure 6 for HeLa mitochondria.

Supplementary Discussion 1: pH change estimation

A detailed estimate of the pH change measured using the graphene electrode with tethered mitochondria shows that our devices are much more sensitive than commercial pH meters. The intimate contact between the mitochondria and the graphene leads to dramatically enhanced sensitivity of the graphene conductance to small changes in pH, even above and beyond the sensitivity in the “bulk pH change” calibration curve (Fig. 2c). Therefore, the sign of the conductance change indicates acidification or alkalization, but the magnitude of the conductance change (although not quantitatively calibrated) is a much more sensitive measurement of pH than existing commercial pH meters (see below).

Estimate of # of protons per mg of mitochondria taken up during CCCP induced depolarization:

Based on the commercial pH meter measurement, the measured pH change in the bulk suspension of mitochondria can be used to determine the # of protons taken up per mg of mitochondria upon introduction of CCCP.

We apply the Henderson-Hasselbalch equation and account for the movement of protons. In the case of CCCP where a net loss of protons to the mitochondrial inner membrane space, the equation is as follows:

$$pH = pKa + \log \frac{[A^-]}{[HA]} \quad (1)$$

$$\Rightarrow \Delta pH = \log \frac{n_{A^-} + n_{H^+}}{n_{HA} - n_{H^+}} - \log \frac{n_{A^-}}{n_{HA}} \quad (2)$$

A^- : weak acid

HA : conjugate base

n_{HA} : original moles of the weak acid and its conjugate base

n_{H^+} : moles of protons loss from the buffer

The KCl buffer contains 2 mM HEPES as the majority buffer with a pKa of 7.5. The original buffer pH is 7.2. In the bulk suspension experiments, 200 μ g of mitochondrial protein in 2 mL volume induces a pH change from 7.21 to 7.23 after the addition of CCCP (as measured by the commercial pH electrode). Hence, the number of protons transferred to the inner membrane space is 20.7 pmoles/0.1 μ g.

In the tethered mitochondria experiments, we used 0.1 μ g of mitochondrial protein in a 50 μ L volume. If we estimate the # of protons taken up based on the bulk measurements above, such

a quantity of mitochondria would induce a pH change of $\sim 4 \times 10^{-4}$ in the entire 50 μL solution volume, much too small to be measured by commercial pH electrodes. Such a change would also give rise to a small conductance change in the graphene if it occurred in the bulk solution volume (estimated to be 0.001% change from Fig. 2c). However, because of the intimate contact between the graphene and mitochondria, a much larger (few %) change in graphene conductance is measured, indicating the exquisite sensitivity of our devices to mitochondrial induced pH changes compared to existing techniques. A similar analysis in the case of BIM induced release of protons can be carried out, and yields similar conclusions.

Supplementary Discussion 2: pH Resolution

Other pH sensors based on field effective sensing and nano-material have been demonstrated¹⁻³. From the Nernst equation, the theoretical sensitivity of a pH sensing surface is around 60 mV/pH. Our computed sensitivity is 8 mV/pH. This limit is, however, not directly related to the detection limit of the platform. The detection limit cannot be computed without accurate noise measurements⁴. To complicate that matter further, while higher sensitivity in terms of mV/pH is generally desired for higher pH resolution, lower mV/pH lowers the charge threshold for detection⁵. Collectively, while the pH sensitivity of semiconducting materials and graphene are promising in biosensing applications, the criterion to assess their performance is still a matter of further research.

Supplementary Discussion 3: The quantity of mitochondria loaded vs. the quantity estimated in each assay

It is worth noting that we used 40 μL of 0.14 $\mu\text{g}/\mu\text{L}$ mitochondrial protein (determined by BCA protein analysis) of HeLa isolated mitochondria. The quantity of mitochondrial protein loaded to a graphene device was then $\sim 5.6 \mu\text{g}$. After the incubation and wash steps, unbound mitochondria were certainly washed away so we estimated the mitochondrial protein that was tethered by using the density of particles observed from MitoTracker \rightarrow Green FM fluorescence. We claimed this estimated quantity (0.1 μg in the report) is the quantity used by one experiment even though we loaded a higher quantity at the beginning. We would insist that this claim is reasonable because that was the actual quantity of mitochondria used by one experiment. The loading of isolated mitochondria at the beginning can be optimized and we suspect that loading 0.1 μg would yield similar amount of tethered mitochondria requiring a slightly altered parameter such as loading time.

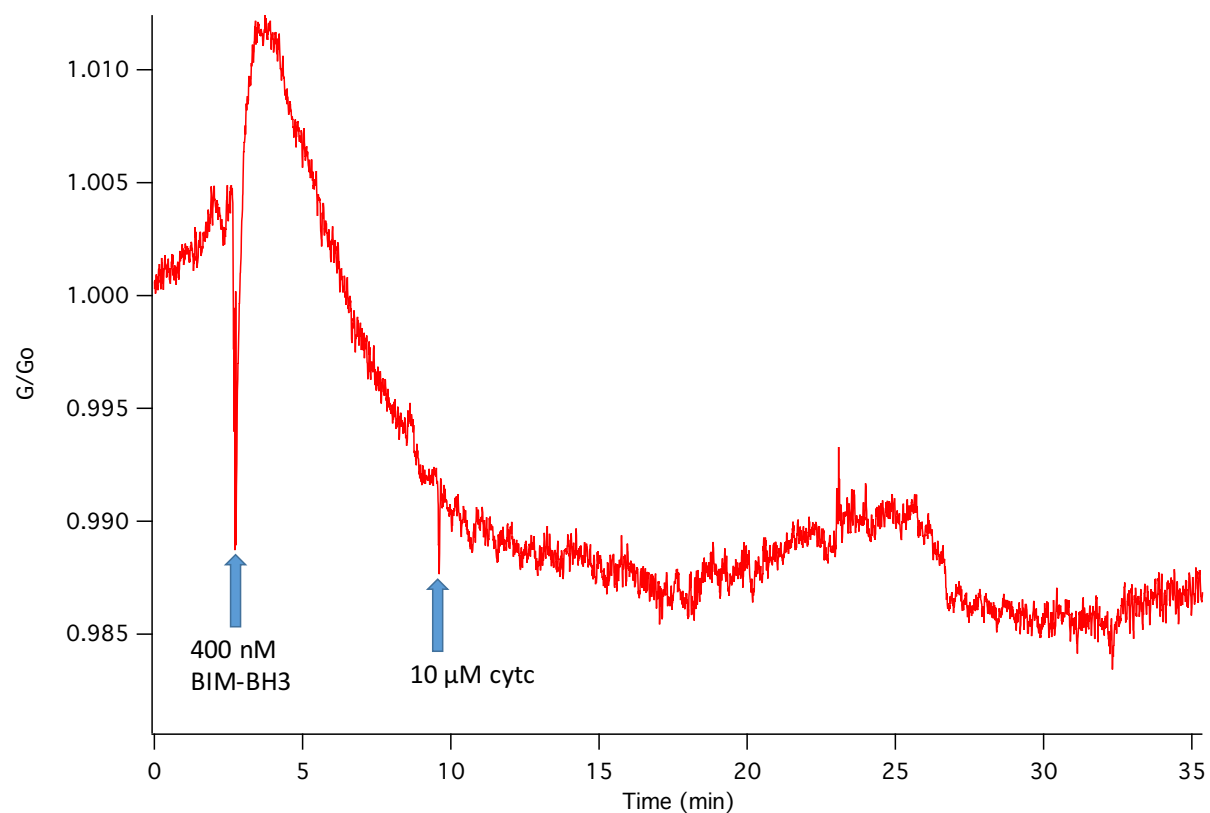
Supplementary Discussion 4: The role of cardiolipin peroxidation during MOMP in buffer acidification

A second order effect concerning cardiolipin peroxidation may contribute to and enhance the observed buffer acidification, although its relative contribution to the effect is hard to estimate quantitatively. Cardiolipin is a proton trap, and hence may serve as a “reservoir” of protons at the inner membrane⁶. However, during MOMP, peroxidation of cardiolipin⁷ can release its

trapped protons to the intermembrane space and hence the buffer, causing additional buffer acidification.

Supplementary Discussion 5: Concentrations of peptides

For the majority of the experiments, the peptide concentration was kept at 100 μM . Although this concentration is standard for BH3 profiling method^{8,9}, due to the amount of assayed mitochondria in this study (100 pg), peptide BIM-BH3 (at 100 μM = 9 μg) may oversaturate the outer membrane and the graphene surface. Therefore, we tested 400 nM of BIM-BH3 (0.036 μg) in inducing MOMP in HeLa mitochondria.



Supplementary Figure 9: Addition of a lower concentration of BIM (400 nM) still reduce the graphene conductance, indicative of acidification. Addition of external cytc stabilized the conductance, evident of loss of acidification. HeLa cells mitochondria were used in this experiment.

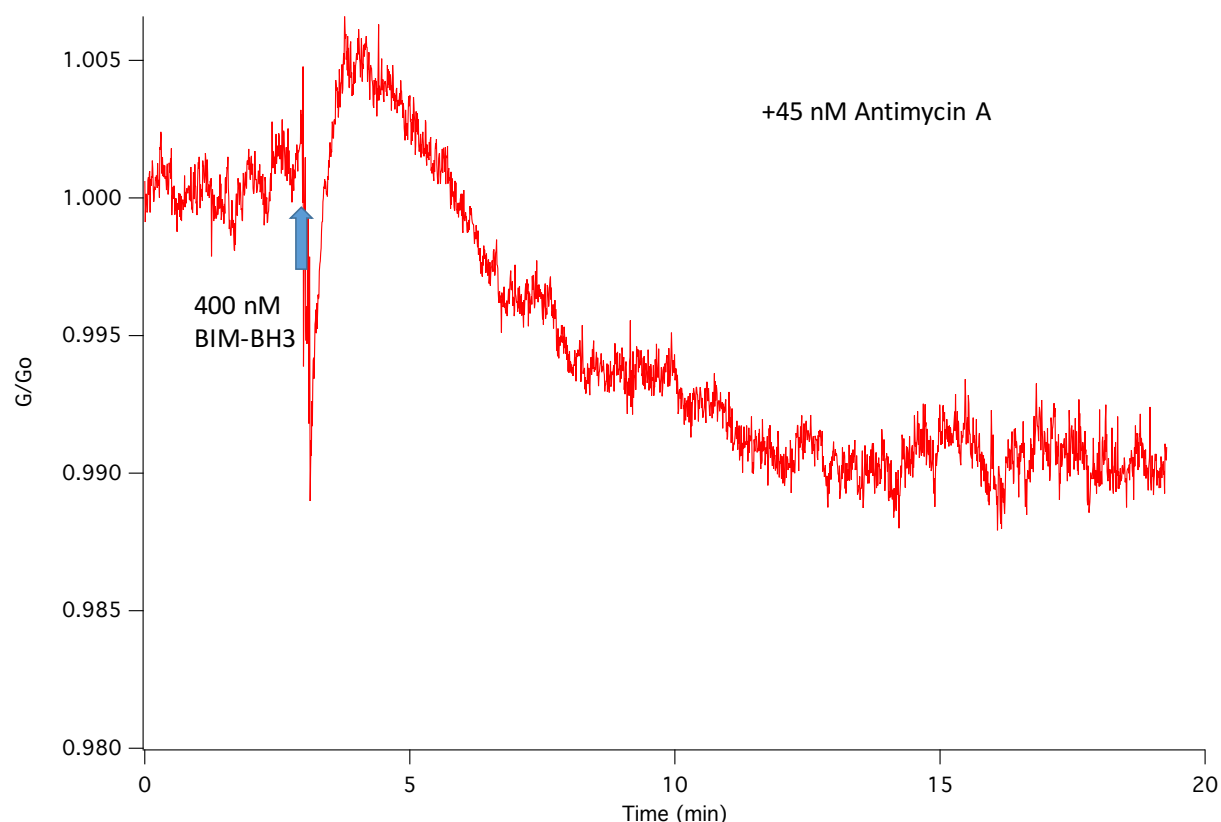
Supplementary Figure 9 shows that 400 nM BIM is still effective in reducing the graphene conductance, suggesting acidification.

Supplementary Discussion 6: exogenous cytc added before or after BIM addition has no effect on acidification

Supplementary Figure 9 shows the results where we added exogenous cytc after BIM addition to check if we could rescue acidification. After cytc, the graphene conductance reduced at a slower rate and eventually fluctuate around a straight line, indicative of acidification rescue. Similarly, in Figure 4b of the main text, we showed rescue of graphene conductance decrease (or acidification) when exogenous cytc had been included in the experimental buffer.

Supplementary Discussion 7: ROS production does not affect graphene conductance

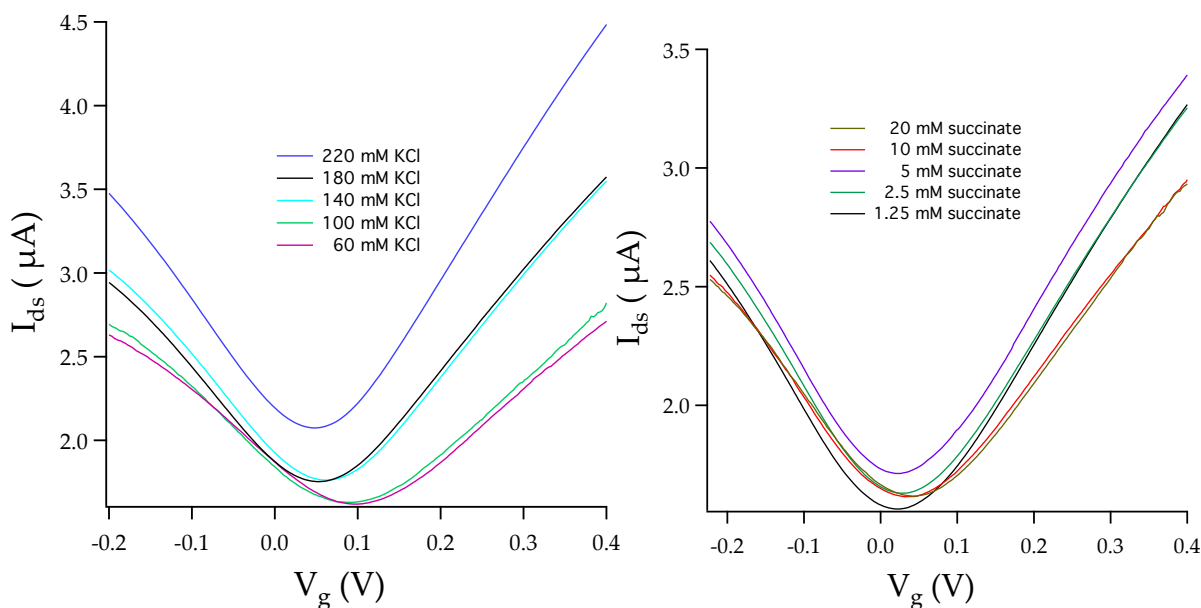
Our experimental buffer contained 5 mM succinate as a carbon source for the mitochondria and we also included limit rotenone to block ROS production by complex I. Nevertheless, complex III is also a major source of ROS, which could affect our pH measurements. When cytc is released following MOMP blocked complex III is stalled and thus can start to produce ROS. To investigate if ROS produced by complex III has any effect on acidification, we used 45 nM Antimycin A to our KCl buffer to block complex III. Supplementary Figure 10 shows that inclusion of Antimycin A did not block the conductance reduction by BIM-BH3.



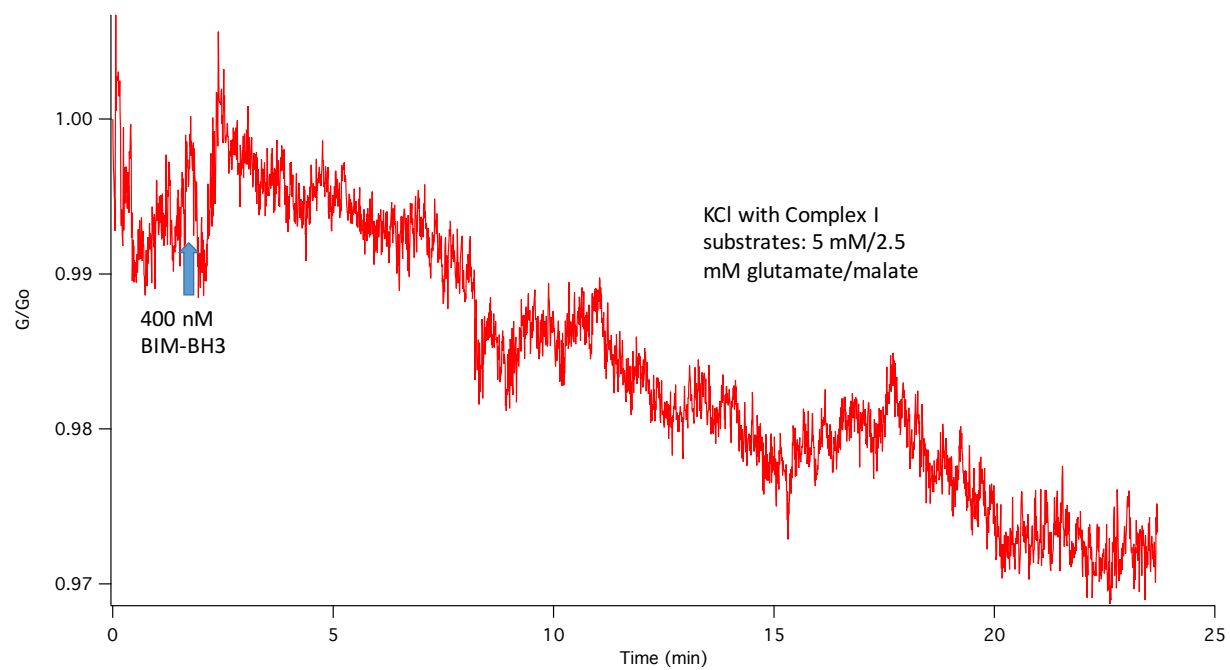
Supplementary Figure 10: Inclusion of 45 nM antimycin A in the experimental buffer did not affect the onset of graphene conductance decline (or acidification). HeLa cells mitochondria were used.

Supplementary Discussion 8: Functionalized graphene sensitivity to other ions other than protons

In Fig. 2d, we showed that the graphene's conductance stable following the addition of 1 μM CCCP, 100 μM BIM-BH₃, and 10 μM cytc (final concentrations). Additionally, mitochondria exchange and consume charged species with the buffer, which in principle may also cause changes in the graphene conductance. In particular, potassium fluxes likely occur during mitochondrial permeabilization, while succinate is a weak acid whose diffusion and consumption could contribute to the local pH changes. Therefore, we tested the response of our functionalized graphene to potassium and succinate (Supplementary Fig. 11). For potassium, at 0 V gate voltage, a concentration change of order 100 mM is required to change the graphene conductance by 10%. Because potassium concentration in our experimental buffer is 140 mM, it is unlikely that the potassium fluxes during mitochondrial permeabilization caused any significant current change. Similarly, for succinate, we found that a 10 mM change in succinate concentration would be required to change the graphene conductance by 10% (Supplementary Fig. 11). In our respiration buffer, the mitochondria were kept in State 4 (no ADP, so very little consumption of substrates is expected). Therefore, the consumption of succinate is unlikely to have caused significant change in graphene conductance or local pH. Although it is impossible with existing technology to estimate (or even identify) all of the charged metabolic substrates released by permeabilized mitochondria, because of the low sensitivity of graphene to potassium and succinate, we can assume that other metabolites also do not change the graphene conductance significantly.



Supplementary Figure 11: For potassium, at 0 V gate voltage, a concentration change of order 100 mM is required to change the graphene conductance by 10%. Similarly, for succinate, we found that a 10 mM change in succinate concentration would be required to change the graphene conductance by 10%.



Supplementary Figure 12: We also performed an experiment with complex I substrates 5mM glutamate/2.5 mM malate in KCl buffer. 400 nM BIM addition causes a reduction in graphene conductance (or acidification). HeLa mitochondria were used.

References:

1. Gao, X. P. A., Zheng, G. & Lieber, C. M. Subthreshold Regime has the Optimal Sensitivity for Nanowire FET Biosensors. *Nano Lett.* **10**, 547–552 (2010).
2. Ferrer-Anglada, N., Kaempgen, M. & Roth, S. Transparent and flexible carbon nanotube/polypyrrole and carbon nanotube/polyaniline pH sensors. *Phys. Status Solidi Basic Res.* **243**, 3519–3523 (2006).
3. Mailly-Giacchetti, B. *et al.* pH sensing properties of graphene solution-gated field-effect transistors. *J. Appl. Phys.* **114**, 084505 (2013).
4. Rajan, N. K., Routenberg, D. a & Reed, M. a. Optimal signal-to-noise ratio for silicon nanowire biochemical sensors. *Appl. Phys. Lett.* **98**, 264107–2641073 (2011).
5. Gao, X. P. A., Zheng, G. & Lieber, C. M. Subthreshold Regime has the Optimal Sensitivity for Nanowire FET Biosensors. *Nano Lett.* **10**, 547–552 (2010).
6. Haines, T. H. & Dencher, N. a. Cardiolipin: A proton trap for oxidative phosphorylation. *FEBS Lett.* **528**, 35–39 (2002).
7. Kagan, V. E. *et al.* Cytochrome c acts as a cardiolipin oxygenase required for release of proapoptotic factors. *Nat. Chem. Biol.* **1**, 223–232 (2005).
8. Ryan, J., Brunelle, J. K. & Letai, A. Heightened mitochondrial priming is the basis for apoptotic hypersensitivity of CD4⁺ CD8⁺ thymocytes. *Proc. Natl. Acad. Sci.* **107**, 12895–12900 (2010).
9. Letai, A. *et al.* Distinct BH3 domains either sensitize or activate mitochondrial apoptosis, serving as prototype cancer therapeutics. *Cancer Cell* **2**, 183–192 (2002).